

Evaluation of synthesis variables on the morphology and mesoscopic order of mesoporous titania films and their photocatalytic activities

Master of Science Thesis in the Master Degree Program Materials and Nanotechnology

Ning Yuan

Department of Chemical and Biological Engineering
Division of Applied Surface Chemistry
CHALMERS UNIVERSITY OF TECHNOLOGY
Göteborg, Sweden 2012

Evaluation of synthesis variables on the morphology and mesoscopic order of mesoporous titania films and their photocatalytic activities

Master of Science Thesis in the Master Degree Program Materials and Nanotechnology

Ning Yuan



Supervisors: Anders Palmqvist & Björn Esbjörnsson
Examiner: Anders Palmqvist

Department of Chemical and Biological Engineering
CHALMERS UNIVERSITY OF TECHNOLOGY
Göteborg, Sweden 2012

Evaluation of synthesis variables on the morphology and mesoscopic order of mesoporous titania films and their photocatalytic activities

Ning Yuan

© Ning Yuan, 2012

Department of Chemical and Biological Engineering
Chalmers University of Technology
SE-412 96 Göteborg
Sweden

Telephone +46 (0) 31-772 1000

Cover: TEM image of mesoporous titania film prepared from a microemulsion aged at 40 °C for 1 hour.

Department of Chemical and Biological Engineering
Göteborg, Sweden 2012

Abstract

Photocatalysis of TiO₂ has been deeply studied in areas of water splitting and decomposition of organic compounds. All these studies are based on the excitation of electrons from valence band of TiO₂ to its conduction band. As the area of nanotechnology develops, new types of nanomaterials become available with improved photocatalytic properties of TiO₂ due to e.g. their large surface area, low rate of recombination of charge carriers, and adjustable band gap.

In this project, ordered mesoporous TiO₂ films were synthesized at low temperature and different parameters that could affect the morphology and crystallinity of the materials were also studied in order to investigate the synthesis process of this type of TiO₂ thin films and the relations between synthesis variables and photocatalytic activities.

A microemulsion containing Pluronic F-127, ethanol, HCl aqueous solution and titanium butoxide was introduced and aged at 40 °C in an oven. Then it was spin-coated on glass slides to form thin films. The films were aged at room temperature and different humidity environments. The photocatalytic activity was monitored by UV-Vis spectroscopy following the degradation of phenol under certain illumination by UV light. The effects of different aging time of the microemulsion in the oven were investigated. Transmission Electron Microscopy (TEM) and Scanning Electron Microscopy (SEM) were applied to detect the morphology and crystallinity of the samples aged for different periods of time. From the results it can be concluded that all the films have a mesoporous structure. However, an ordered hexagonal mesoporous structure can only be achieved with the aging time of the microemulsion below 48 hours. All ordered films contain crystallites with a size between 2-5 nm. The concentration of crystallites is higher for films prepared using longer aging time. The sample aged for 96 hours does not show an ordered mesoporous structure but it contains the highest amount of crystallites and the crystallite size grows up to 10 nm or above. The photocatalytic activities linearly increase as the aging time of the microemulsion is extended, which may result from the increasing content of crystallites and the bigger crystallite size.

The effects of humidity during the aging phase of TiO₂ films were also studied. Grazing-incidence small-angle X-ray scattering (GISAXS) and SEM were used to investigate the order of the mesoporous structure. The results show that the higher the humidity was, the better the order of the pores was. This might be because the certain humidity can sustain fluidity of the system, which is necessary for the self-assembly behavior of surfactant. GISAXS also shows information about porosity and pore size, which are generally getting higher and bigger,

respectively when the applied humidity increases. TEM and UV absorption figures also show that films aged at lower humidity contain fewer crystallites, which results in lower photocatalytic activity.

Finally, the effects of iron dopant were briefly evaluated. For this material, a relatively low content of iron dopant could enhance the photocatalytic activity. Excess iron dopant could even diminish the photocatalytic activity of the mesoporous TiO₂ films.

Keywords: Photocatalysis, Ordered mesoporous TiO₂ films, Microemulsion, Crystallite, aging time, humidity, Iron dopant.

Contents

ABSTRACT	4
INTRODUCTION.....	8
THEORY.....	10
SURFACTANTS AND THEIR SELF-ASSEMBLY BEHAVIORS	10
MESOPOROUS MATERIALS	11
MICROEMULSION	12
BAND GAP OF SEMICONDUCTORS	13
QUANTUM SIZE EFFECT	13
PHOTOCATALYSIS PHENOMENON OF TiO ₂	14
EFFECTS OF DOPANT.....	16
PHOTOCATALYTIC DECOMPOSITION OF PHENOL.....	17
ANALYTICAL TECHNIQUES.....	18
UV-Vis SPECTROSCOPY	18
TEM.....	19
SEM.....	20
GISAXS.....	20
EXPERIMENTAL METHODS.....	23
CHEMICALS.....	23
METHODS	23
Spin coating	23
Storage condition for aging	23
FABRICATION OF ORDERED MESOPOROUS TiO ₂ FILMS.....	24
Synthesis of crystalline TiO ₂ in microemulsion	24
Reaction.....	24
Formation of ordered mesoporous TiO ₂ films	25
Aging of TiO ₂ films at different humidity environments	26
Formation of mesoporous TiO ₂ films with Fe dopant	26
Photocatalytic activities of ordered mesoporous TiO ₂ films.....	27
CHARACTERIZATIONS	28
TEM.....	28
SEM.....	28
UV-Visible spectroscopy	29
GISAXS	29
RESULTS AND DISCUSSION.....	30
SERIES OF MESOPOROUS TiO ₂ FILMS PREPARED AT DIFFERENT AGING TIME	30
Morphology	30
UV-Vis Absorbance.....	35
Blank experiment	35

Photocatalytic activity measurements	35
HUMIDITY SERIES.....	37
Morphology	38
UV-Vis transmission measurements	42
Photocatalytic activity measurements.....	44
FE DOPANT SERIES	46
Photocatalytic activity measurements.....	46
CONCLUSIONS.....	48
FUTURE WORK	49
ACKNOWLEDGEMENT.....	50
REFERENCES.....	51

Introduction

Phenol and its derivatives are widely used in chemical industries. The waste of them would cause lots of serious environmental problems, such as reducing or inhibiting biodegradations of other components in water,^[1] so it is very important to eliminate or reduce the concentration of phenol to a safe low level. Traditional ways include physical adsorption on activated carbon^[2] and advanced oxidation processes by introducing strong reducing agent working with ultraviolet light to produce hydroxyl radicals.^[3-5] The drawbacks of the former way are slow processing at high concentration and contaminations are just transferred but not eliminated. The degradation for the second way is efficient, however the reducing agents available here are very expensive.^[1]

As renewable and green energy resources aroused great interest from the middle of last century, photocatalytic effects of TiO₂ also became intriguing and were greatly developed from the early part of last century. For example, the study of photo-bleaching of dyes by TiO₂ powders was reported in 1938.^[6] Japanese scientists Honda and Fujishima first discovered that water can be split by shining light on TiO₂ in 1972.^[7] About the same time, people also started to pay attention on applying TiO₂ photocatalysis to organic pollution clean-up and it has been proved to be very effective and practical by the high activity and low cost of TiO₂.^[8]

As nanotechnology developed, the size of the TiO₂ materials was reduced to nano-scale, such as nano TiO₂ powders or mesoporous TiO₂ films which could give much higher activity compared with the bulk materials due to very high surface area of TiO₂ and lower rate of charge carriers' recombination. Mesoporous materials contain pores with diameter between 2 nm to 50 nm. Materials with such structure are well applied for catalysis, sorption, sensors, ion exchange, photovoltaics.^[9-12] The arrangement of the pores in mesoporous structures can be either ordered or disordered according to the synthesis conditions. The materials themselves can be crystalline or amorphous. Ordered arrangement of pores is normally formed under wet chemical condition by introducing surfactants as template, which can be easily removed afterwards.^[13]

Titania has three main polymorphs, including anatase, rutile, and brookite. In the case of photocatalytic applications, anatase was proved to be the most effective.^[14] Temperatures over 350 °C are typically required for crystallization of titania through solid state reactions,^[15-16] which is difficult to control and mesoorder could be broken down easily as the particles grow.

Lately, a new method of synthesizing the mesoordered anatase at low temperature with tunable size of crystallite was reported by Nilsson et al.^[17]

In this project, the photocatalytic activity of this new material was studied by decomposing phenol in aqueous solution, Different parameters, such as aging conditions for different phases and the addition of dopant, that could affect the morphology and the photocatalytic activity were also investigated, as well as the possible mechanisms.

Theory

Surfactants and their self-assembly behaviors

Surfactants are amphiphilic molecules containing hydrophilic head groups favoring water phase and hydrophobic tails which usually are hydrocarbon chains favoring oil phase (see figure 1). They are most commonly used for reducing the surface tension of liquids, interfacial tension of different liquids or that between liquid and solid. Due to their special properties, they can be used as detergents, emulsifier, foaming agent and so on. Generally, surfactants can be divided into three categories: cationic, anionic, nonionic according to their molecular structures, especially the head groups.^[18]

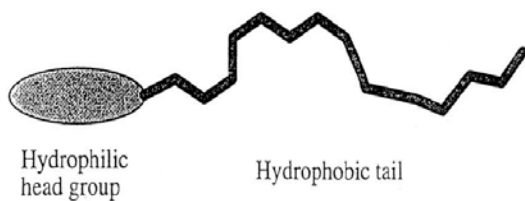


Figure 1. Typical structure of a surfactant molecule (figure adapted from ref. 18).

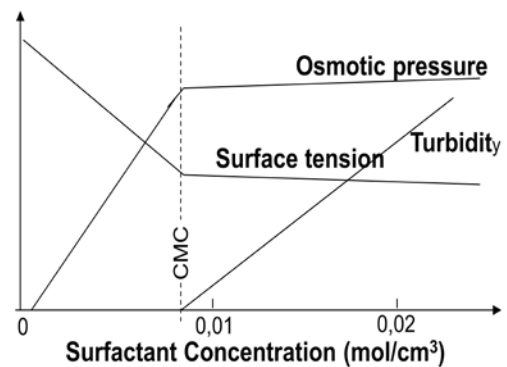


Figure 2. The physical-chemical properties of a solution at the CMC (figure adapted from ref. 19).

The behavior of surfactant aggregation consists of three main steps as the concentration goes up continuously (see figure 3). First, at low concentration of surfactants in solutions, surfactant molecules distribute at the surface and interface of different phases as free molecules. Head groups are in the water phase, tail groups are in the oil or air phase. Small amounts of free molecules dispersed in the solution. Second, as the concentration increases over a certain level, there is no space at the surface and interface for more free molecules, and the extra surfactants cannot sustain free in the solution and therefore start to interact and aggregate forming micelles. In this way, the free energy of the system decreases. This turning point is called critical micelle concentration (CMC). Each kind of surfactant has its own CMC where many physical-chemical properties change (see figure 2). Surfactant aggregates have different shapes due to different critical packing parameter (CPP) of surfactants which determines the shapes of the surfactant aggregates, such as spherical micelle, cylindrical micelle, bilayer, and reversed micelle. Third, as the concentration keeps increasing, the

volume fraction of micelles will be too high for the micelles to exist randomly in the solution. They thus begin to form liquid crystals with long range order to lower the energy of the system. Depending on the CPP and concentration of surfactants, different shapes of liquid crystals can be formed.^[18]

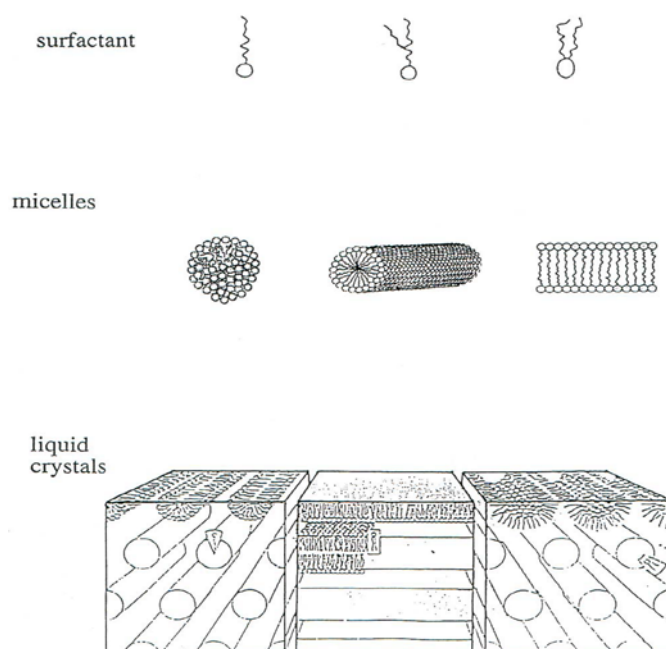


Figure 3. The behaviors of different surfactants as their concentration increases (figure adapted from ref. 19).

Mesoporous materials

Mesoporous materials are materials with a porous structure where the pores have diameters between 2 to 50 nm. If the arrangement of the pores is ordered in a crystalline lattice, such as cubic or hexagonal, then the materials are called ordered mesoporous materials (see figure 4). Different pore arrangements can give different properties to the materials. Synthesis of mesoporous materials typically needs templates which are formed by the proper surfactants based on their self-assembly behaviors. The materials are subsequently formed in a coassembly process with the templates. Finally, the templates can be removed by burning or (in the case of photocatalytic materials) by degrading under illumination with UV light, which leaves the materials with a mesoporous structure.^[20]

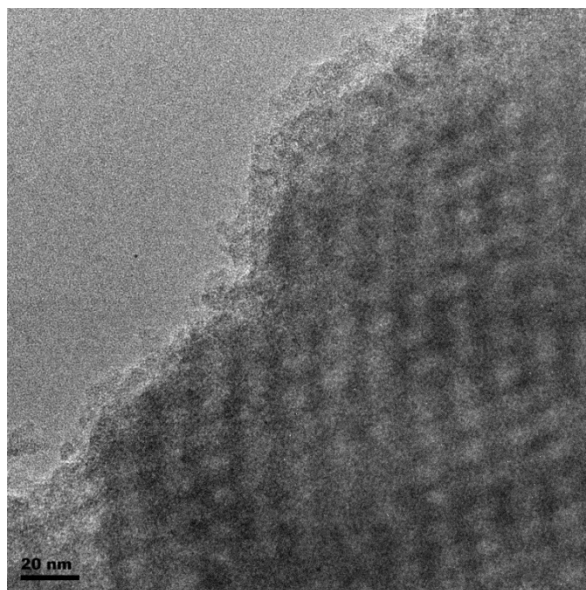


Figure 4. Ordered mesoporous TiO_2 with hexagonal arrangement of pores from this project.

Microemulsion

Microemulsions are thermodynamically stable mixtures consisting of individual domains of oil and water, which are separated by a monolayer of surfactants (see figure 5), Microemulsions have diameters about 10 nm and large internal surface. If water is the continuous phase where oil droplets are dispersed, this is named oil in water (o/w) microemulsion. If oil is the main component where water droplets are dispersed, it is called inverted (w/o) microemulsion. The dispersed droplets can provide isolated reaction volumes for either organic or inorganic reagents to form nanoparticles due to the continuous fusion/reformation and diffusion of droplets, from which the reactants can come in contact with each other and react.^[18]

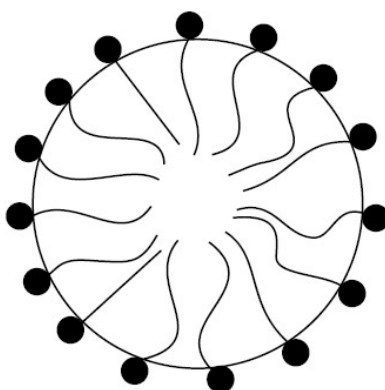


Figure 5. Typical structure of oil in water microemulsion (figure adapted from ref. 18).

Band gap of semiconductors

The term band gap, also called energy gap, represents an energy range in a material where no electrons can exist according to the theory of solid state physics. It generally refers to the energy difference between the top of the lower energy level, referred to as the valence band, and the bottom of the higher energy level, referred to as the conduction band, where the electron states can exist. Only when electrons are in the conduction band can they move freely and conduct electricity. So the band gap decides a lot of properties of solid state materials. If the band gap is too large, it is very hard for electrons in the valence band to be excited to the conduction band. Such materials are generally called insulators. If the band gap is smaller, the electrons in the valence band can more easily acquire enough energy from outside, such as photons or heat, and be excited to the conduction band, where they can move freely. This type of materials is called semiconductors. If the band gap is too small or the valence band and conduction band overlap, electrons can always conduct electricity and such materials are called conductors.^[21] Figure 6 shows the band gap differences among these three materials.

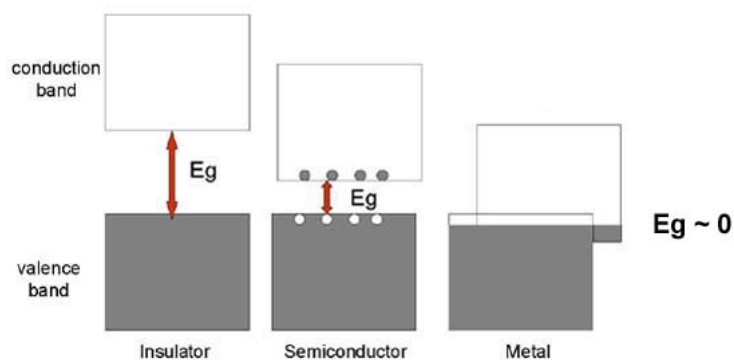


Figure 6. Schematic band gap diagrams for an insulator, a semiconductor, and a metal (figure adapted from ref. 22).

Quantum size effect

Quantum size effects of nanomaterials are based on the confinement of the movement of electrons when the size of materials reaches nanometer scale. This results in discrete energy levels and changes the properties of materials. In the case of a semiconductor crystallite, an increase of the valence-conduction band gap E_g results as the diameter (D) of the nanocrystallite decreases. The relation between band gap expansion of nanometric semiconductor and their crystallite size can be described by function of $\Delta E_g(D) = E_g(D) - E_g(\infty)$, Δ and ∞ represent the change and bulk size, respectively. The dependence of quantum-sized semiconductor's band gap on particle size can be described by figure 7.^[23] The smaller

crystallite contains fewer atoms and fewer molecular orbits and has a larger band gap. By considering this effect, many properties of materials can be varied by adjusting their size.^[24]

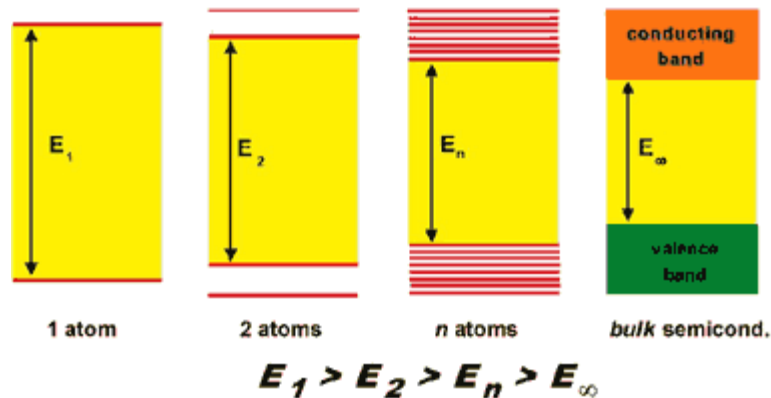


Figure 7. Schematic diagram of quantum size effect (figure adapted from ref. 23).

Photocatalysis phenomenon of TiO₂

Photocatalysis is a process in which typically semiconductors are used to absorb the energy from electromagnetic radiation in the form of photons to generate species that have very high reactivity and are able to induce reactions of chemicals. Plank's equation reveals the relation between the frequency, ν , of the electromagnetic radiation and the associated energy, E , and is expressed as follows,

$$E = h \nu, \quad (h \text{ is the Plank's constant}) \quad (\text{Equation 1})$$

TiO₂ is a common semiconductor which has a band gap of 3.2 eV. This corresponds to the energy of radiation with a wavelength about 387.5 nm. When TiO₂ is irradiated with light with a wavelength under 387.5 nm, which means the energy of the radiation is higher than the band gap energy of TiO₂, TiO₂ will absorb the energy from the photons to excite the electrons in the valence band to the conduction band, creating positive charged holes (h_{vb}^+) in the valence band and free electrons in the conduction band (e_{cb}^-). Figure 8 describes the process of photocatalysis of TiO₂. The specific reactions during this process are also explained by equation 2.

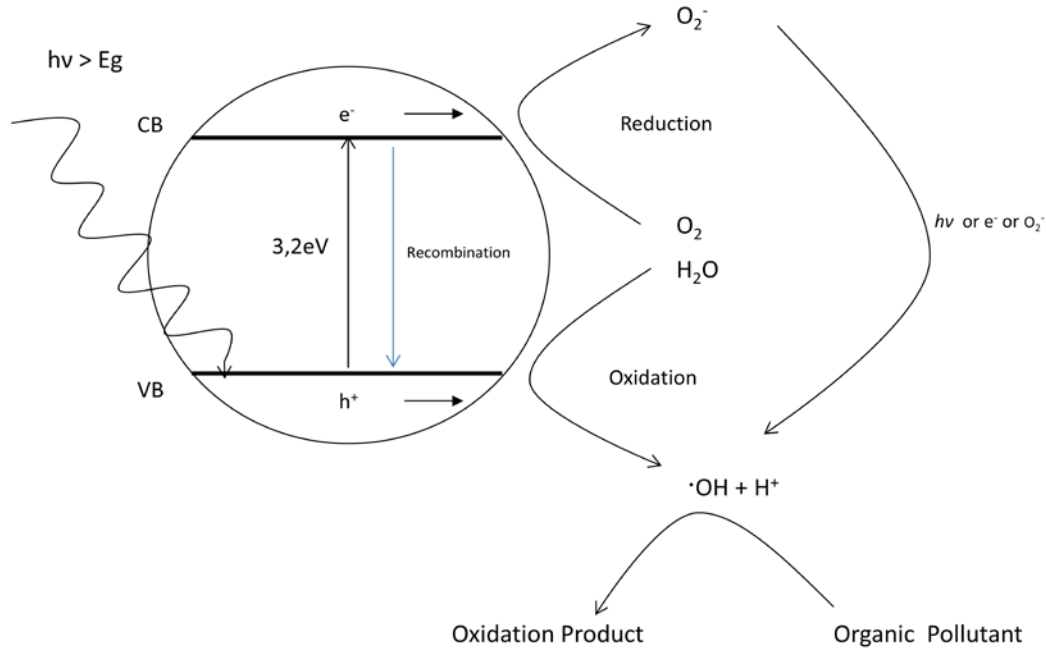
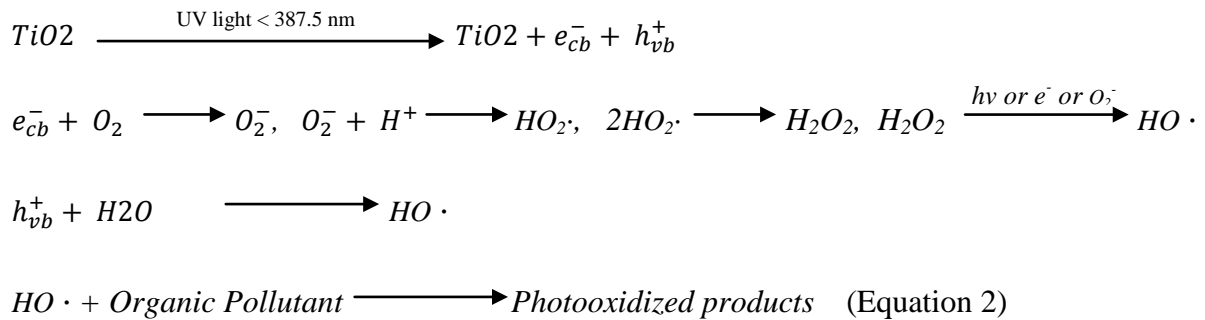


Figure 8. Schematic diagram of TiO₂ photocatalysis process for degradation of organic pollutant.



The free electrons interact with oxygen yielding superoxide radical anions. The positive charged holes interact with water yielding highly reactive hydroxyl radicals, which are well known for oxidizing most organic pollutants and giving final products of CO₂ and H₂O.

In most cases, the lifespan of the free charge carriers are very short due to their high reactivity and instability. The recombination of e⁻-h⁺ pairs can inhibit the photocatalytic efficiency of the semiconductor resulting in the dissipation of heat and light. The recombination can proceed both inside the materials and on their surface. One of the most effective ways to minimize the recombination rate of e⁻-h⁺ pairs is to reduce the size of the particles to the nano

scale. Since the smaller the size is, the higher surface-to-volume ratio can be achieved, and the diffusion length of the e^-h^+ pairs from the interior of the materials (such as the wall of mesoporous materials) to their surface can be greatly reduced and they can compete with the surface recombination. At the same time, a larger surface area can give more positions for more reactants to be adsorbed and interact with charge carriers on the surface efficiently instead of recombining together.^[25]

Effects of dopant

To improve the photocatalytic efficiency of TiO_2 further, one approach is to modify it so it absorbs more light, resulting in increased formation of charge carriers. To achieve this target, the surface area of the materials and the size of the crystallites can be adjusted to optimum levels. Another efficient method is to introduce dopants. Dopants can be either metals, such as Fe, Cu,^[26-28] or nonmetals, such as N, C.^[29-31] Since every element has their own set of energy levels for electrons, when dopants are introduced, they will result in the formation of new energy bands incorporated into the band gap of TiO_2 . The new incorporated band can be divided into two types. If they are close but lower than the conduction band of TiO_2 , they can accept the electrons excited from the valence band of TiO_2 . If they are close but higher than the valence band of TiO_2 , they can donate their own electrons to the conduction band. Due to the less energy separation between the incorporated bands and the conduction band or valence band, longer wavelengths of light can be absorbed producing more charge carriers and performing better photocatalytic activities.^[25]

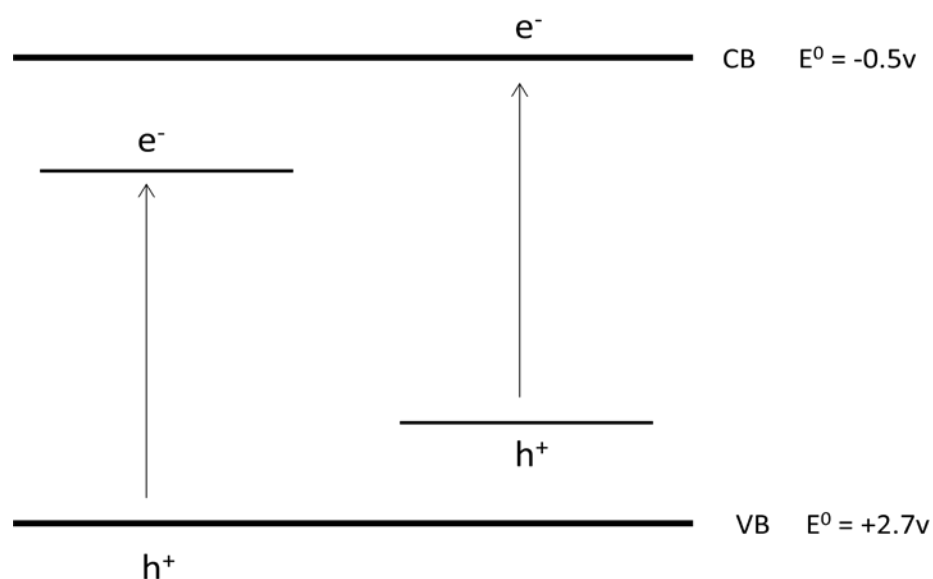


Figure 9. Schematic diagram of the incorporated bands created by dopants (figure adapted from Ref. 32).

Photocatalytic decomposition of phenol

Photocatalytic decomposition of phenol may proceed via different pathways which produce different byproducts. Hydroxyl radicals are usually considered to be the main oxidizing agent generated by the photocatalytic action of TiO_2 . Equation 3 illustrates the reaction of complete decomposition of phenol. Two different mechanisms including intermediate products are proposed in Figure 10.^[33,34]

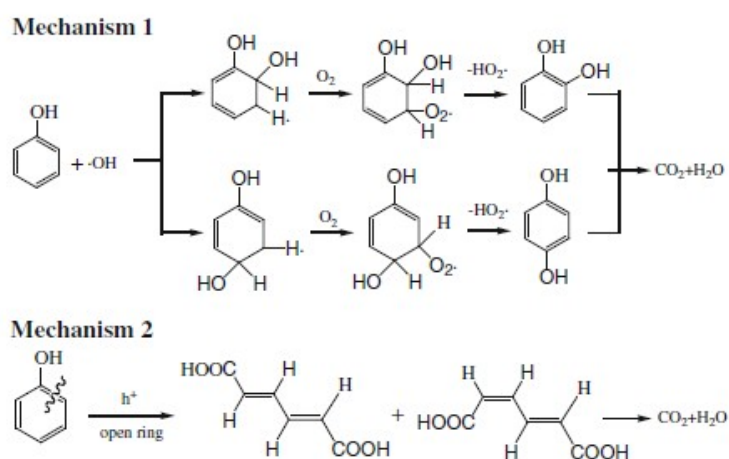


Figure 10. Two proposed mechanisms of photocatalytic degradation of phenol (figure adapted from Ref. 34).

Analytical Techniques

UV-Vis Spectroscopy

UV-Vis spectroscopy (Ultraviolet-visible spectroscopy), is a technique that is mainly used for measuring the absorbance of ultraviolet-visible light by organic molecules. This technique is based on Lambert-Beer's law which reveals the relationship between absorbance and concentration of an absorbing species. Lambert-Beer's law is written as $A = a(\lambda) * b * c$, where A is the absorbance, $a(\lambda)$ is a wavelength-dependent absorptivity coefficient, b is the path length of light, and c is the sample's concentration. Experimental measurements are carried out by introducing transmittance (T), which is defined as $T = I / I_0$, where I is the light intensity after passing through the sample and I_0 is the initial light intensity. The relation between A and T can be illustrated as $A = -\log T = -\log (I / I_0)$.^[35]

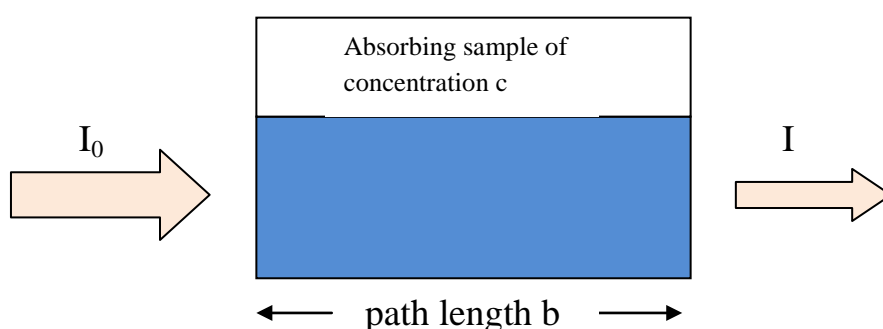


Figure 11. Schematic illustration of Lambert-Beer's law (figure adapted from Ref. 35).

When molecules absorb certain amount of energy from radiations, the electrons in the lower energy orbits of the molecules will be excited to higher energy orbits. For different molecules, their energy differences are unique, which can be used as a standard to identify molecules. UV-Vis spectroscopy can also quantitatively measure the radiation absorbance at certain wavelength, which indicates the concentration of a species in a solution.

The absorbance of light in the ultraviolet-visible spectra region of solid state materials, such as solid thin films, can also be used to measure the band gap of semiconductors, or the characteristics of multi-layer films.^[36]

TEM

TEM (Transmission Electron Microscopy) is one of the most important techniques to characterize the morphology of nanomaterials and study the crystallographic information of a crystalline material. The left picture of figure 12 describes the structure and different components of a typical TEM. A beam of electrons are used to characterize the test subjects. Electrons are emitted from the electron gun on the top of TEM and then they are accelerated in a vacuum electron cannon to obtain a certain energy. The electromagnetic lenses are used to focus the electrons to either a small dot or to a rather large area. Finally, the electrons will pass through the samples and form different types of images containing the information of the samples.^[37] The right picture of figure 12 describes the interactions between the incident electron beam and a sample. These interactions can give different signals which can be detected by the detectors. They can provide different and specific information about the sample. Since the electrons have very short wavelength and high energy, TEM can reach a very high resolution which is normally up to nanometer scale. By taking advantage of high-resolution transmission electron microscopy, even higher resolution and the crystallographic information of a sample at an atomic scale can be achieved.

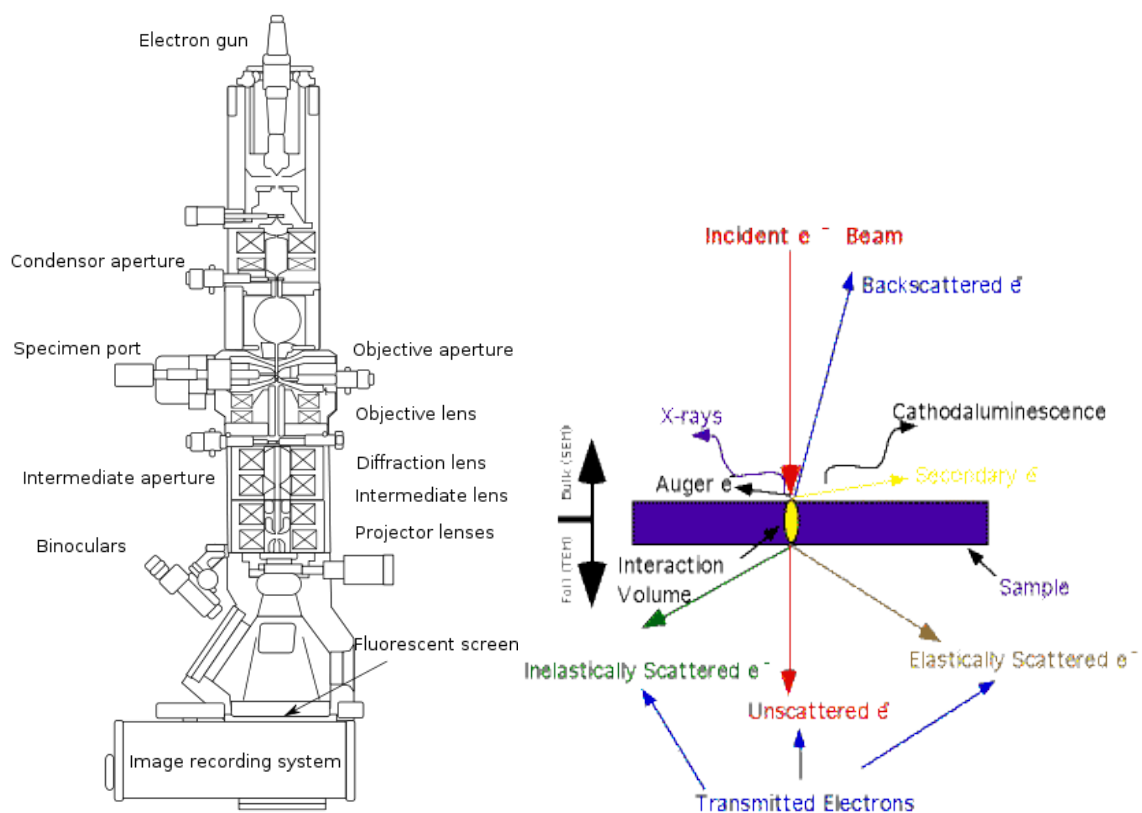


Figure 12. (left) The structure and different components of TEM (figure adapted from Ref. 38). (right) The interactions between the incident electron beam and the sample (figure adapted from Ref. 39).

SEM

SEM (Scanning Electron Microscopy) is another important type of electron microscopy beside TEM. It's typically used to investigate the topography, morphology, composition and crystallographic information of the samples by scanning across their surfaces with high-energy electron beam. Normally SEM has lower resolution compared to TEM, but the higher electron beam energy can still provide resolution of 1.5 nm. When the electron beam strikes the surface, a cascade of electrons in different forms are scattered in all directions which gives different information of the sample's surface. The scattered electrons can be both elastic and inelastic. The elastic electrons generate X-rays and secondary electrons, however, the inelastic electrons are primary. Figure 13 illustrates different kinds of signals that can be achieved and the types of information that a SEM can provide.

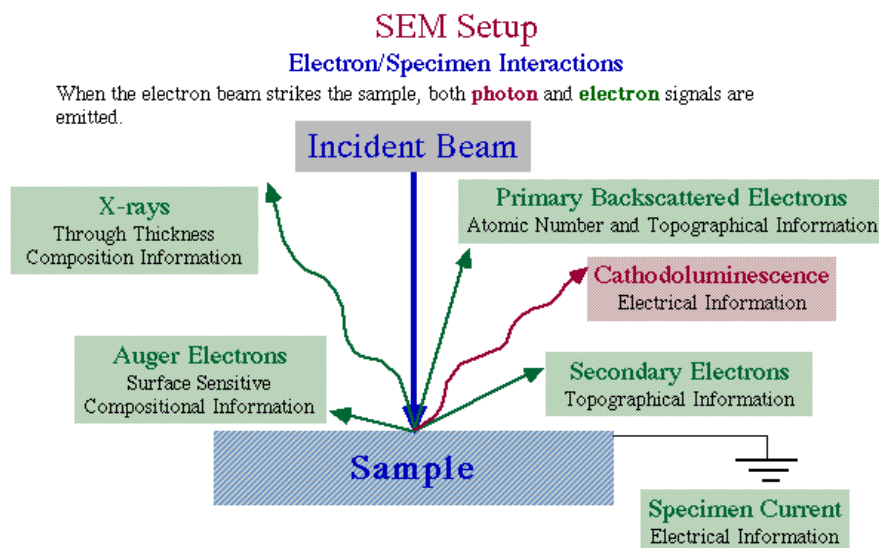


Figure 13. Interactions between incident electron beam and the sample (figure adapted from Ref. 39).

GISAXS

GISAXS (Grazing-incidence small-angle x-ray scattering) is a newly developed technique that is specially used for determining the surface morphologies of samples in nanoscale and internal morphologies and electron density fluctuations of the studied materials. It compensates the limitations of direct imaging techniques that have very small observable area and incapability to determine buried and internal structures.

By taking advantage of smaller beam size with very narrow divergence, scattering experiments can improve the angular resolution. Especially for the study of coatings, thin films and particles on surface, GISAXS is better compared to transmission scattering techniques. Even for thin films within nanoscale thickness, a highly intense scattering pattern can be still formed. Owing to the smaller angle, the x-ray beam path length through the film plan is sufficient, from a few to hundreds of nanometers. Spin- or dip-coating, drop-casting or sputtering techniques are common sample preparation methods.^[40]

The high surface sensitivity of x-ray scattering of GISAXS results from the special chosen grazing incidence angle α (see figure 14), which is in the range of half the critical angle α_c to several times of α_c of the thin film materials. Depending on the materials to be studied, specific grazing incidence angle will be chosen. When free-standing quantum dots are being studied, incidence angle below critical angle is preferable to achieve highest surface sensitivity of x-ray scattering. When the incident angle is between critical angle of the thin film and the substrate, largest scattering cross sections can be reached. In this case, multiple scattering effects should be considered in order to model the data correctly. Dynamic scattering effect is largely diminished when the incident angle is over the critical angle of the substrate, which facilitates the model of data within the quasi-kinematic approximation.^[41]

The scattering intensity of scattered rays over a range of exit angles β and scattering angles ψ in the surface plane are recorded by the area detector. With purpose to hinder spillover direct beam and reflected beam, a beam stop needs to be set up, resulting in a simple scattering geometry and capability to study in-situ environment of samples. Real-time study can also be carried out due to the high scattering intensity in the forward direction.^[42]

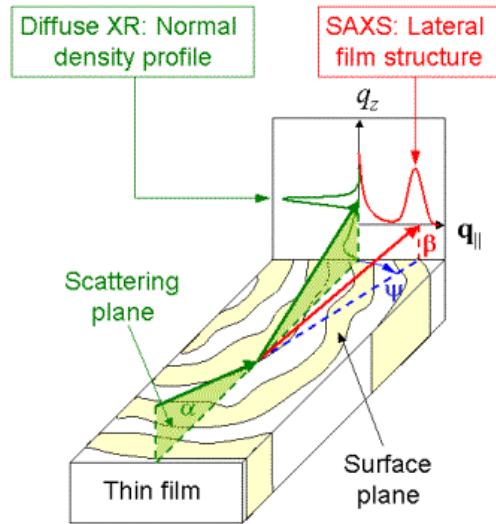


Figure 14. Schematic diagram of the principle and different parameters of GISAXS (figure adapted from Ref. 41).

Experimental Methods

Chemicals

Titanium(IV) butoxide (97%), Pluronic F-127 ($M_w = 12600$) were purchased from Sigma-Aldrich. Ethanol (99.5%) was purchased from Solveco. Milli-Q water (resistivity 18.2 M Ω .cm) was provided by a Millipore “Milli-Q plus” unit.

Methods

Spin coating

Spin coating is a time and cost efficient way to fabricate homogeneous thin films on different substrates. It involves three steps (see figure 15). First, deposit coating materials on the center of the substrate. Second, rotate the substrate in certain speeds to spread the coating materials by centrifuge force. This process normally includes two phases. The first phase usually has low speed and lasts for short time with the purpose of spreading the coating materials across the whole substrate. The second phase has higher speed and works longer time with the purpose of removing extra materials and forming homogeneous thin films. The solvent evaporates during this process. Finally, the homogeneous thin films form on the substrate. The film-forming process is primarily driven by two independent parameters – viscosity of the solvent and spin speed. Lower viscosity and higher rotating speed give thinner films. As the solvent evaporates, not only the films become thinner, but also the materials may change their morphology in micro-scale, such as the microemulsion system.

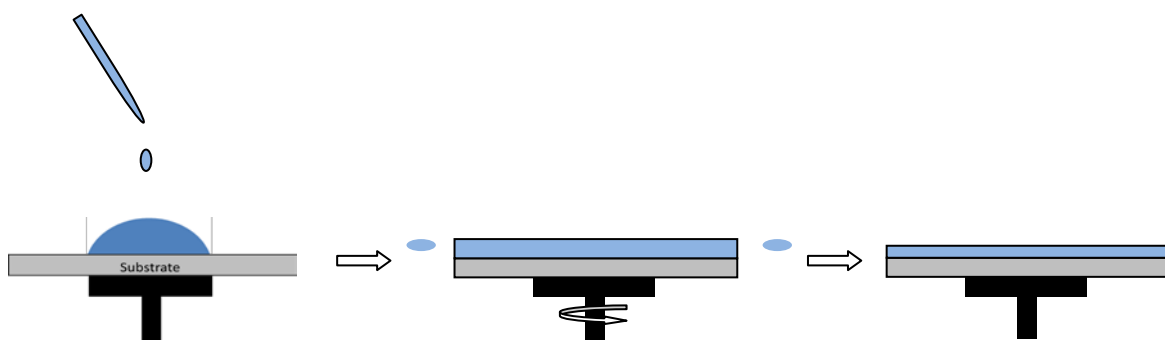


Figure 15. Stages of spin coating process to fabricate thin films.

Storage condition for aging

Figure 16 shows the different aging conditions for thin films after fabricating by spin coating. The left one is a typical sealed bucket containing a beaker with saturated NaCl aqueous

solution in order to create the environment of about 75% relative humidity. On the right is the box used to create different humidity environments by containing silica gel which maintains the relative humidity below 5%, and saturated aqueous solutions of different salts. The salts used in this project were LiCl, K₂CO₃, NaCl and K₂SO₄ which can control the inside environment with 21%, 45%, 75%, 98% relative humidity, respectively.



Figure 16. Storage conditions for the aging of TiO₂ thin films.

Fabrication of Ordered Mesoporous TiO₂ Films

Synthesis of crystalline TiO₂ in microemulsion

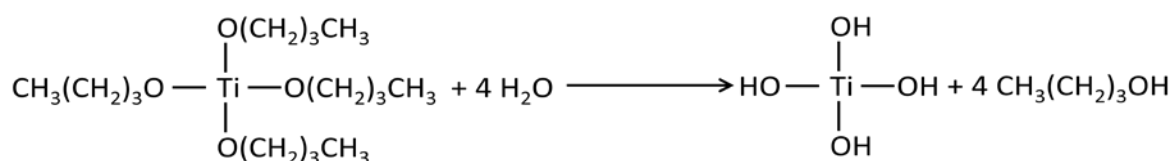
Microemulsion was prepared by mixing certain amount of oil phase and aqueous phase. The oil phase here consists of titanium(IV) butoxide as the precursor of TiO₂ and butanol produced from the hydrolysis reaction of precursor. The aqueous phase here is hydrochloric acid solution. The surfactant here is nonionic ethyleneoxide₁₀₀-propyleneoxide₇₀-ethyleneoxide₁₀₀ triblock copolymer Pluronic F127 (M_w = 12600), and the final mixture had weight proportion of 1:1.5:2:1 of 5 M HCl:F127:ethanol:titanium(IV) butoxide. The microemulsion was prepared by stirring this mixture until it became homogeneous and transparent. Then it was moved into an oven with 40 °C and kept there from 1 h to 96 h for aging. TiO₂ crystallites could be formed in the microemulsion and grow slowly during this phase.

Reaction

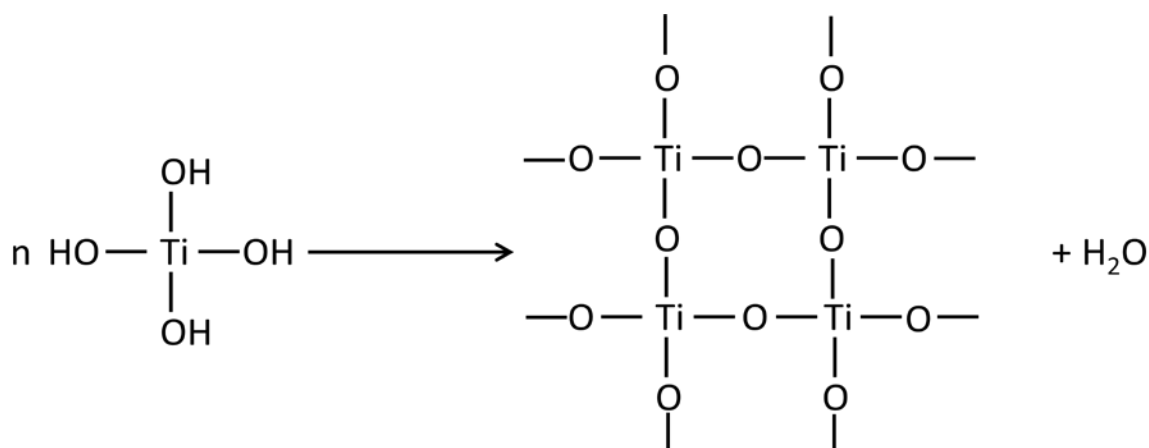
There are two reactions that proceed in the microemulsion system. The first is hydrolysis of the precursor producing Ti(OH)₄ and butanol. This process has a very high reaction rate. Ti(OH)₄ and butanol contribute to the water phase and oil phase of the microemulsion,

respectively. Then $\text{Ti}(\text{OH})_4$ molecules will condense together and lose water molecules to form bigger molecules. If many $\text{Ti}(\text{OH})_4$ molecules condense together, they may form polymeric net structures. This process will give either amorphous or crystalline TiO_2 . However, this process has a relatively lower reaction rate. The equations describe one of the possible specific reaction routes.^[17]

Hydrolysis



Condensation



Equation 3. Hydrolysis and condensation reactions of titania precursors within the microemulsion system.

Formation of ordered mesoporous TiO_2 films

Samples were prepared after storing the microemulsion in the oven for 1 h, 3 h, 6 h, 12 h, 24 h, 48h and 96 h, respectively by spin-coating the microemulsion on glass substrates to form thin films. The spin-coating consisted of two steps, which were 300 rpm for 5 s and then 1000 rpm for 10 s. The microemulsion dropped on the substrate before the start of spinning was approximately 500 μl . After the films were fabricated, they were put into sealed buckets with beakers containing saturated NaCl solution to create constant 75% relative humidity environment and kept at room temperature for aging which should be at least two days. Then,

the organic components and the rest of the solvent in films were removed by exposing them to UV irradiation for at least 12 hours, remaining the mesoporous TiO₂ films on glass slides.

Figure 17 is the phase diagram of the mixture where gradual change in composition of the synthesis mixture can be studied. Ethanol is assumed to act as an oil phase together with butanol formed during the hydrolysis of titanium n-butoxide. The initial composition was at position 1, after hydrolysis of the alkoxide, the composition moved to position 2. As the ethanol and small amounts of butanol and water evaporated during the spin-coating, it moved to position 2b. Further evaporation of ethanol, butanol and water during the aging phase lead the composition moving to the region H₁ where the liquid crystal formed serving as the template for the mesoordered walls of TiO₂.^[17, 43]

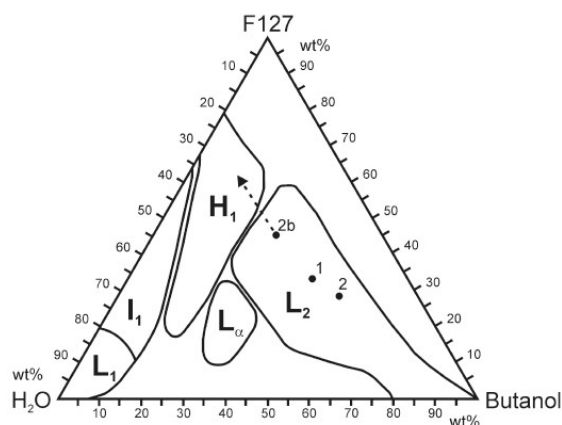


Figure 17. Phase diagram of the synthesis mixture. The initial composition of the synthesis mixture is at position 1. It moves to position 2 during the hydrolysis of the alkoxide. Then the composition of synthesis mixture moves to position 2b as the ethanol and small amounts of butanol and water evaporate during the spin-coating process. Dotted line indicates the expected path of compositional change during the further evaporation of ethanol, butanol and water at the aging phase (figure adapted from Ref. 17).

Aging of TiO₂ films at different humidity environments

4.5%, 12%, 45%, 75%, 98% relative humidity environments for aging phase of TiO₂ films were created by introducing SiO₂ gel, saturated aqueous solutions of LiCl, K₂CO₃, NaCl, K₂SO₄, respectively in a sealed box in order to study how the humidity affects the morphology and photocatalytic activities of the TiO₂ films during the aging phase.

Formation of mesoporous TiO₂ films with Fe dopant

With the purpose to partly replace Ti with other element in the TiO₂ crystallites, certain amount of Fe(NO₃)₃ solutions were added after mixing Pluronic F127, ethanol, titanium(IV)

butoxide and HCl aqueous solution with the same proportion illustrated above. Microemulsions containing 0.4%, 0.8%, 1.2%, 1.6% weight fractions of Fe dopant were prepared. Then follow the same procedures illustrated before to fabricate thin TiO₂ films with iron dopant.

Photocatalytic activities of ordered mesoporous TiO₂ films

Photocatalytic activities of the TiO₂ films were measured by evaluating their ability for degrading phenol under UV radiation. The whole setup for the photocatalytic activity measurement can be seen in the left picture of figure 18. 0.1 mM aqueous phenol solution was used here which was circulated by pumping at a certain speed through the reactor and UV-Visible spectrometer where the concentration of phenol was measured as the reaction proceeded. The reactor has a volume of 4.2 ml. A stable and focused beam was directed on the front window of the reactor. An FTO slide was used here as the shield (see right picture of figure 18) over the front window in order to filter away the light with wavelength below 300 nm which has been shown to lead to the opposite photolysis effect of phenol.^[44] The voltage of the power supply for the lamp was 97 V and the light intensity irradiated to the window between 300 nm to 400 nm was about 430 Watt/m². The TiO₂ films were fixed at the back window in contact with the phenol containing solution. The absolute irradiance spectrum after passing through the FTO slide shield can be seen in figure 19, where we can see the irradiance with wavelength below 300 nm has been effectively eliminated and the total light intensity was mainly contributed by the light with wavelength above 350 nm. The concentration of phenol in the reaction system was measured every 30 minutes during the circulation process, 5 hours in total. The mass of the films was weighed after scraping the films off the glass slides. The photocatalytic activities of the ordered mesoporous TiO₂ films were decided through dividing the degradation fraction of phenol by the mass of the films which varies from 0.39 mg to 0.58 mg.

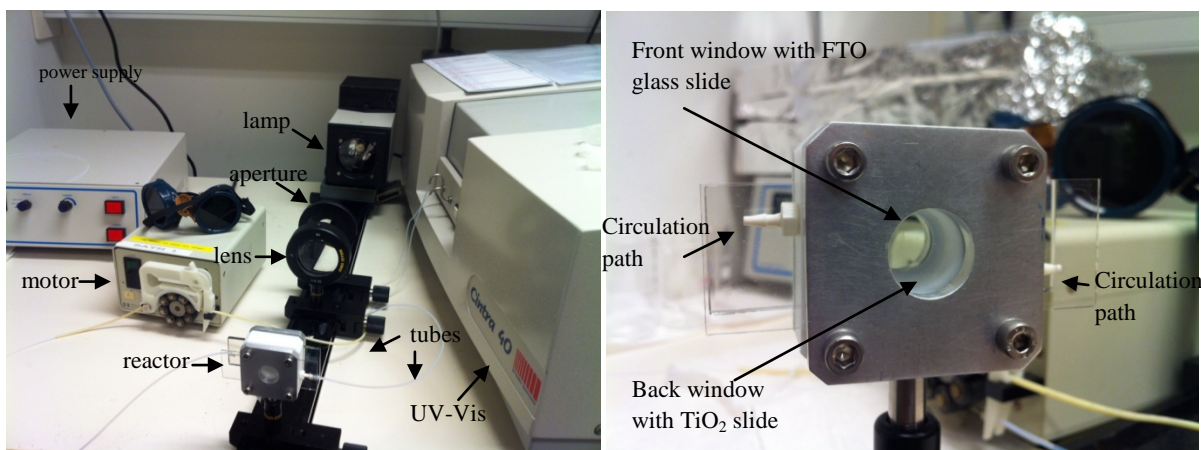


Figure 18. (left) The setup for the photocatalytic activity measurement. (right) The reactor consisting of FTO glass slide and TiO₂ thin film with chamber containing phenol solution in between.

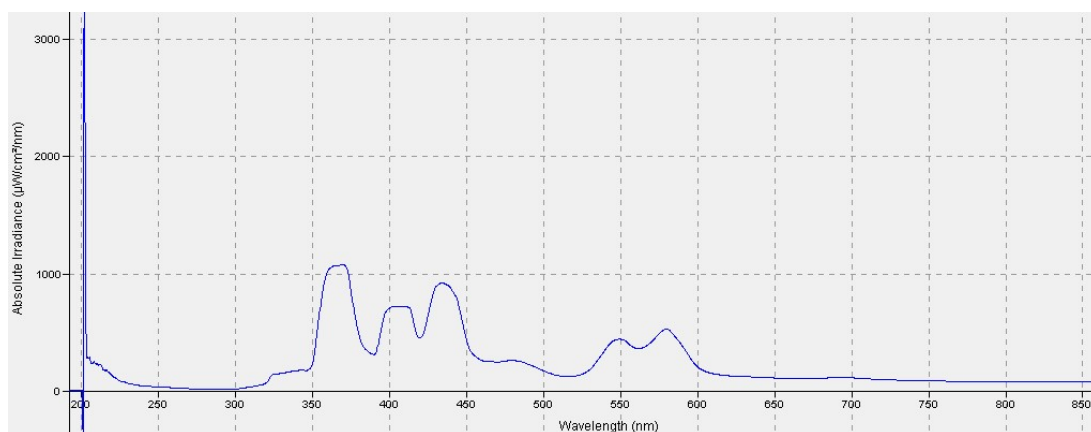


Figure 19. The radiance spectrum irradiating the phenol solution.

Characterizations

HR-TEM

A JEOL JEM-4010 high resolution transmission electron microscopy (HR-TEM) was used in this work as the main approach to characterize the morphology and compositions of TiO₂ thin films. The films after removing organic components were partly scraped off the glass slides and dissolved in ethanol. The solutions were then dropped on the grids and dried for the observation.

SEM

The samples were also investigated by using a JEOL JSM-7600F scanning electron microscopy (SEM) to further study their morphology.

UV-Visible spectroscopy

The photocatalytic activity of TiO₂ thin films was studied by measuring the concentration of phenol in the solutions with a GBC Cintra 40 UV-Visible spectroscopy. Phenol has absorbance peaks of light at the wavelength of 270 nm and 210 nm, respectively (see figure 20). Absorbance at 270 nm was usually used as the standard to decide the concentration of phenol in the reactor. As the phenol was photocatalytically degraded by TiO₂ films, the absorbance signal of phenol from UV-Vis spectroscopy decreased. The degradation fraction of phenol could be calculated via dividing the decreased value of absorbance by the value of its original absorbance after calibration of the curves.

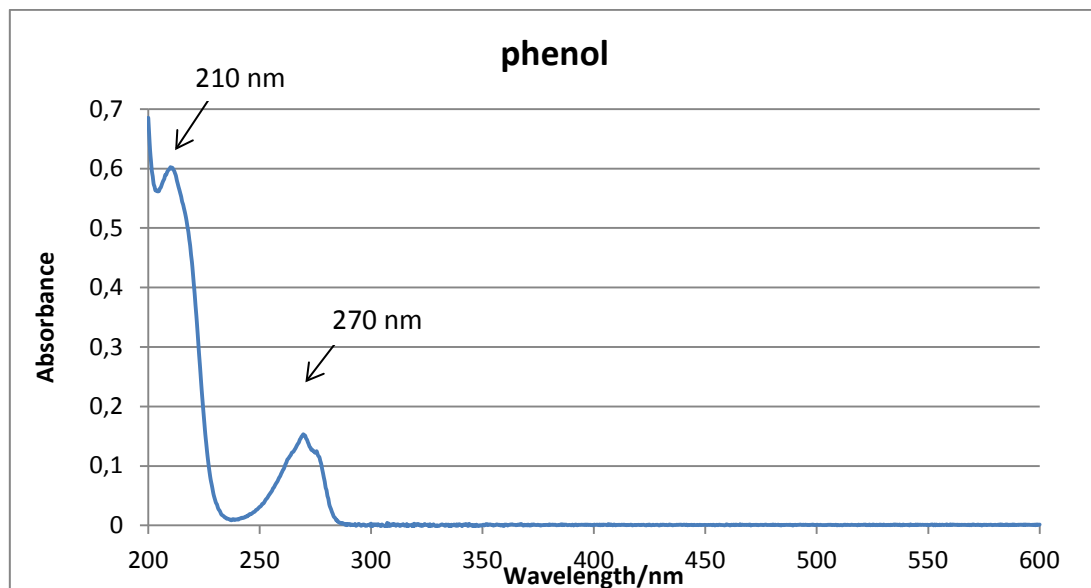


Figure 20. Absorbance of 0.1 mM phenol aqueous solution within the UV-Visible range.

GISAXS

Grazing incidence small angle X-ray scattering (GISAXS) was applied to investigate the morphology of the TiO₂ thin films, including the order of the pores, porosity and the diameter of the pores. The measurements were performed at the MiNaXS beamline P03 at HASYLAB at DESY, Hamburg, Germany.

Results and Discussion

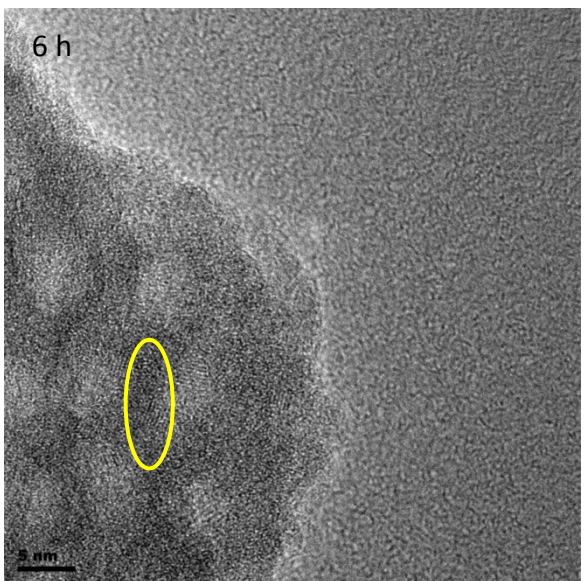
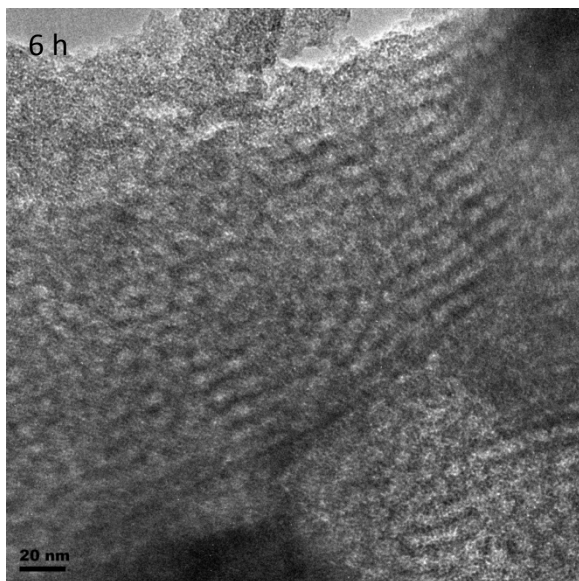
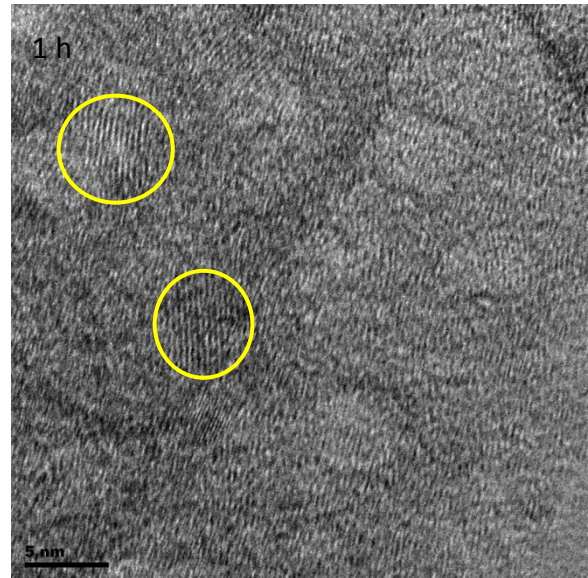
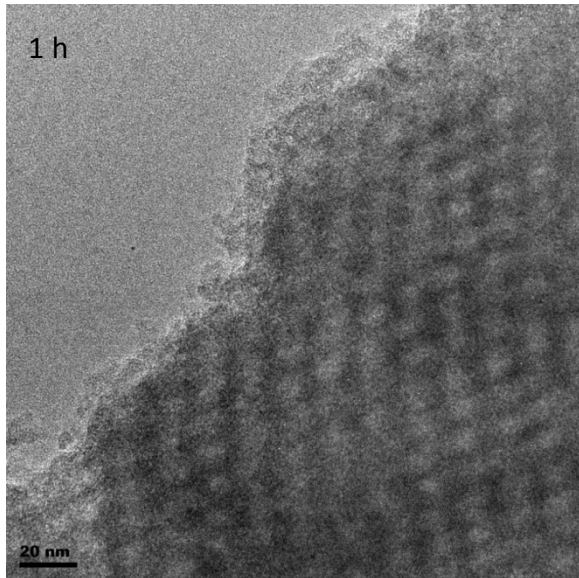
Series of mesoporous TiO₂ films prepared at different aging time

Films of mesoporous TiO₂ were prepared after storing the microemulsion described in the experimental section in the oven for 1 h, 3 h, 6 h, 12 h, 24 h, 48h and 96 h by spin-coating the microemulsion on the glass substrates, then they were aged in sealed buckets with saturated NaCl aqueous solution inside for at least two days. Nanocrystallites of anatase started to form during the aging phase of the microemulsion, and the size of the crystallites also grew slowly in the microemulsion. Different length of aging periods resulted in different amount of crystallites with potentially different size, which could also affect the order of the pores and the photocatalytic activities. This experiment was designed to find the relations among the amount of crystallites, their size, the order of the pores and the photocatalytic activities.

Morphology

Figure 21 shows the morphology of the samples with different aging time for the microemulsion in the oven at 40 °C taken by TEM. The yellow circles marked the representative crystallite areas. From the pictures having scale bars of 20 nm, it can be recognized that 1 h, 6 h, 24 h samples show ordered hexagonal mesoporous structure, and the diameters of the pores are very similar and about 5 nm. The size of crystallites of 1 h, 6 h, 24 h and 48 h samples varies within the range of ca. 2-5 nm. For the sample aged for 96 h, the size of crystallites increases to 10 nm or even larger. Meanwhile, the content of crystallite in the materials for the sample aged for 1 h and 6 h is relatively low and these samples contain large areas of amorphous TiO₂. For the sample aged for 24 h, it can be clearly recognized that there are more crystallites, and the crystallite content continuously goes up for the 48 h and 96 h samples. For 24 h, 48 h, and 96 h samples, crystallites become the main composition of the material. These results indicate that the formation of crystallites started in the microemulsion system, and for relative shorter aging time (below 48 h), the crystallites were not able to grow up to bigger size. However, the longer the aging time in the oven, more crystallites of TiO₂ can be transformed from amorphous TiO₂. This is probably because the TiO₂ polymer molecules acquired more time to relax and find thermodynamically more stable configurations. The proper crystallite size (below 5 nm) could also fit in the pore walls very well, which allowed the materials to maintain the well ordered mesoporous structure. It is reasonable here that the sample aged for 96 h has the highest crystallite content and the crystallites in the microemulsion got enough time to grow bigger to 10 nm. Generally, the

longer the aging time is applied, the more crystallites can be formed, and if the time is long enough, their size can also grow.



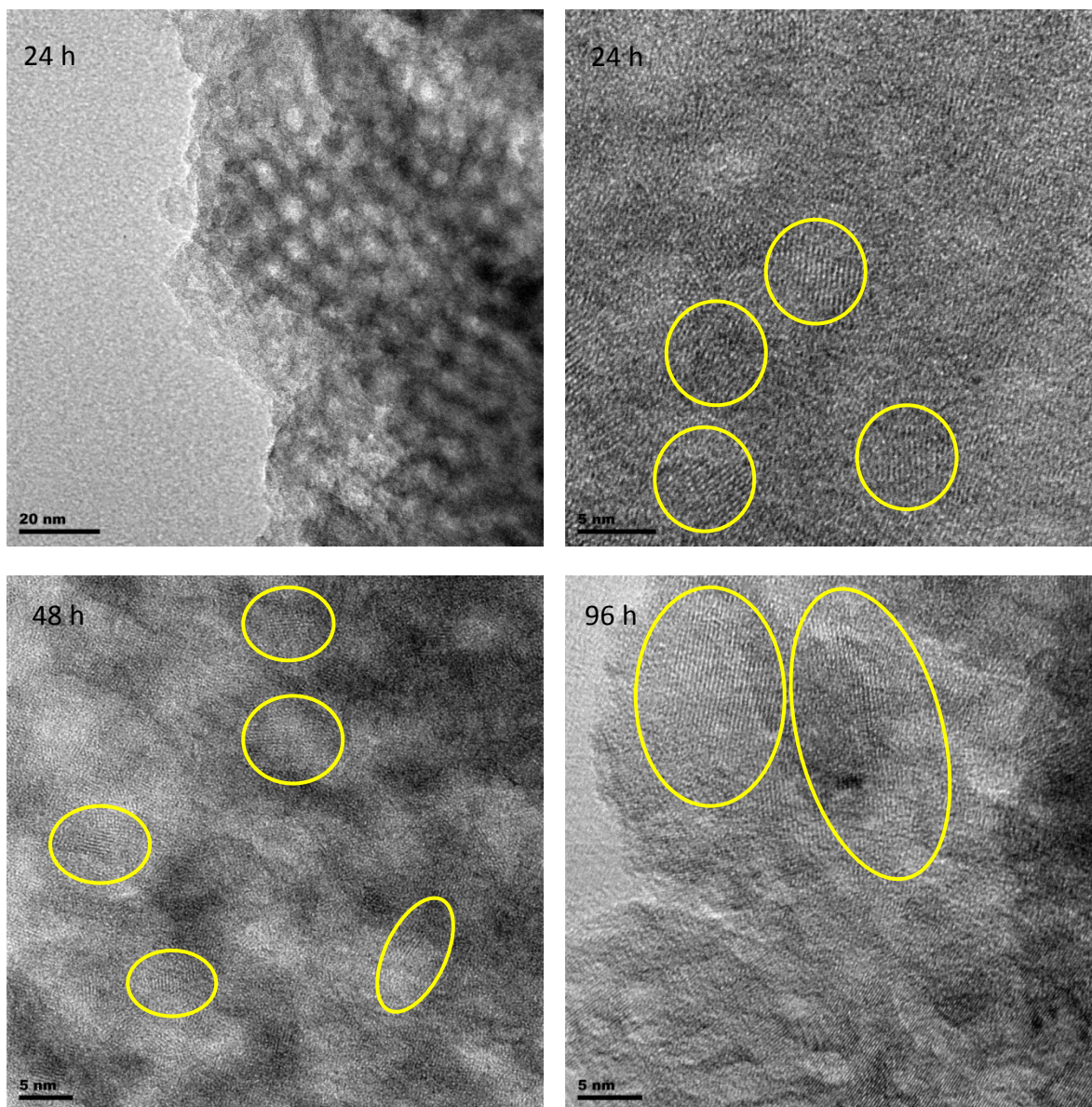
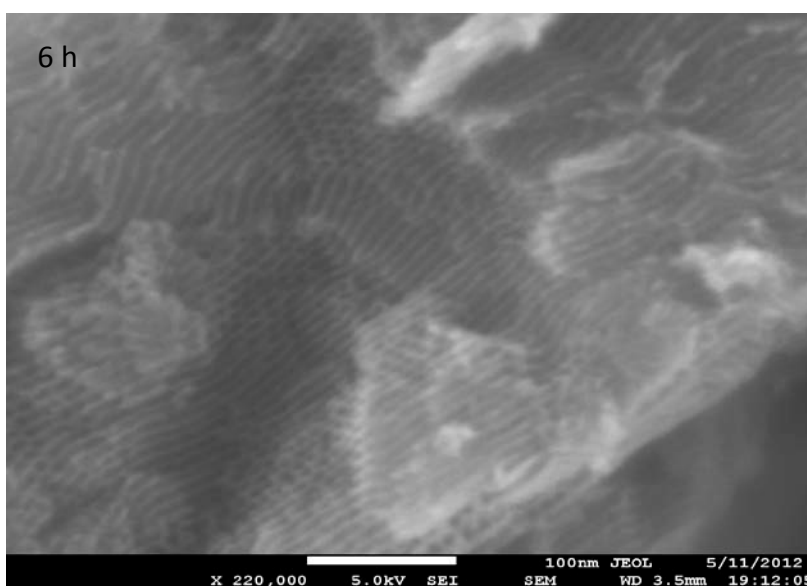
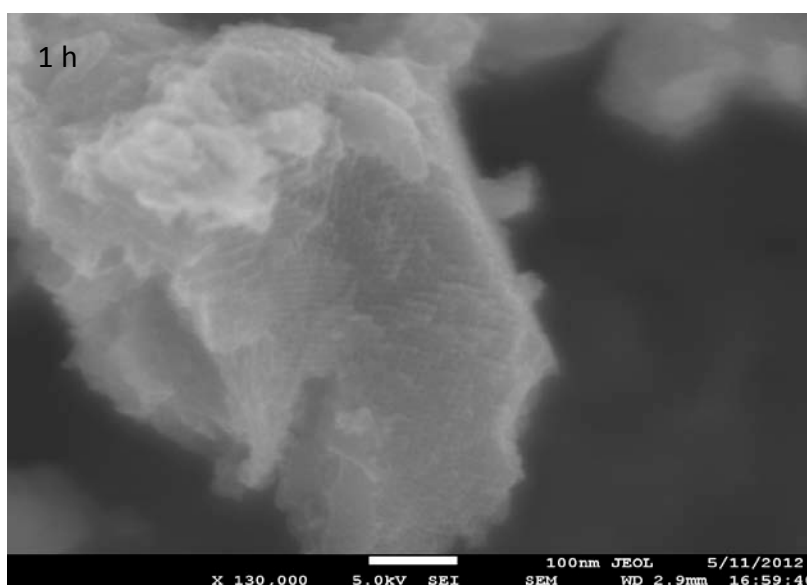


Figure 21. TEM images of TiO₂ films with their microemulsions aged in the oven for different periods of time.

Figure 22 shows SEM pictures of the same series of samples. All the samples show a mesoporous surface structure. Samples aged for 1 h, 6 h, 24 h, 48 h contain pores that align together and are well organized, in what appears to be a hexagonal arrangement. The sample aged for 6 h not only consists of hexagonally arranged porous structures, but also well aligned channels of the pores. The 1 h, 6 h and 48 h samples consist of well ordered hexagonal mesoporous structure in long range. Samples aged for 24h contains shorter range of ordered mesoporous structure, which means in smaller areas, the structure is well ordered. The sample aged for 96 h does not show any ordered mesoporous structure, the shape of the pores is also distorted. These results also correspond with the information from the TEM pictures. By considering the information from the TEM images, the reason why the samples aged for 1 h, 6 h, 24 h, 48 h can achieve the well ordered hexagonal mesoporous structures

with similar crystallite size is because the crystallites were not able to grow bigger than 5 nm in the microemulsion due to the limitation of short aging time. When the liquid crystal template of surfactant formed during spin coating, these crystallites had the proper size to fit into the wall of the porous structure. Then the template performed a restriction for the further growth of the crystallites during the next aging phase of the films. The ordered mesoporous structure and the shape of the pores would sustain and the crystallite size would be restricted to below 5 nm. The disordered mesoporous structure obtained for the sample aged for 96 h is because the crystallites already got enough time to grow up to 10 nm or above in the microemulsion, which was too big to fit in the walls of the pores when the template was formed and the template could not restrict further crystallite growth. This destroyed the ordered mesoporous structure, as well as distorted the shape of the pores.



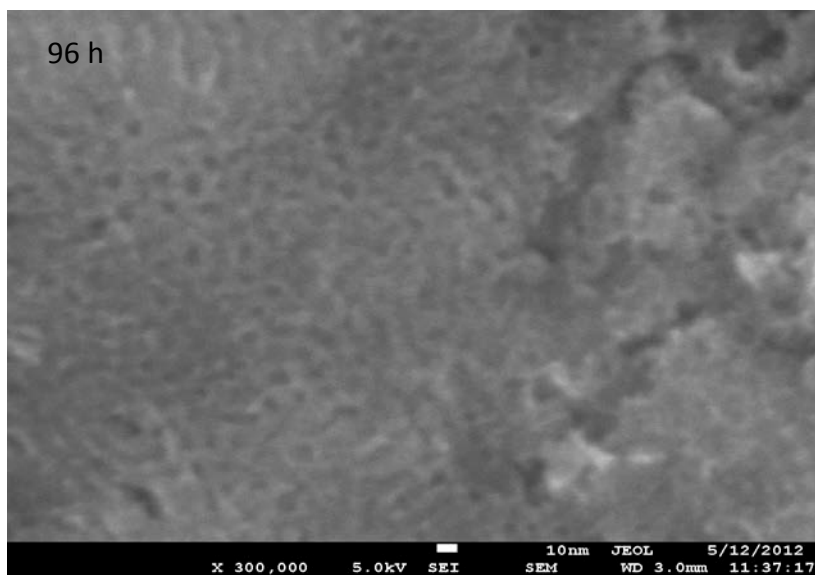
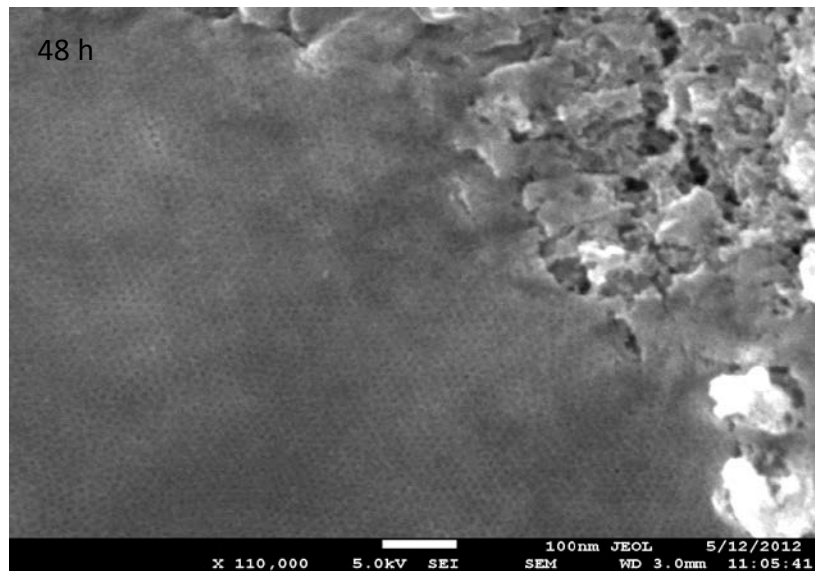
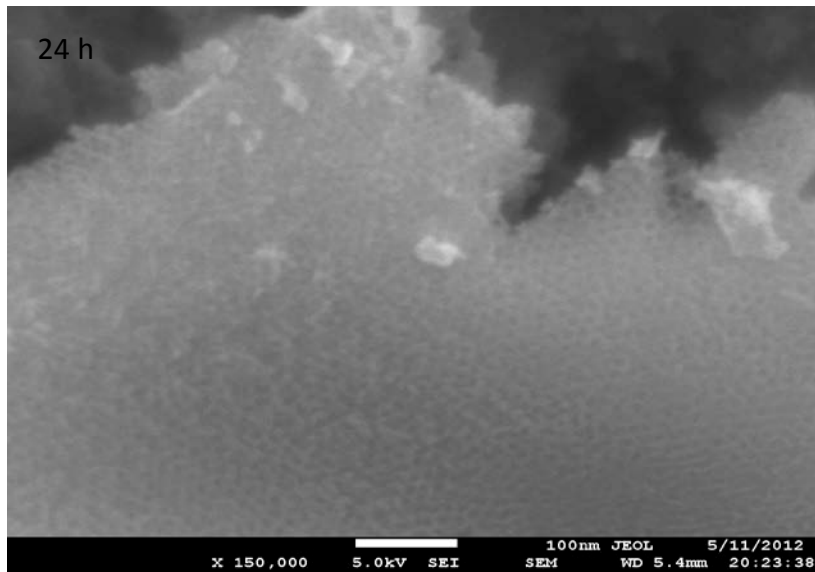


Figure 22. SEM images of TiO_2 films prepared with their microemulsions aged in the oven for different periods of time.

UV-Vis Absorbance

Blank experiment

Figure 23 shows the result of the blank experiment which has the same experimental conditions but used clear glass slide without TiO₂ film on it. As we can see, instead of decreasing, the absorbance at 210 nm and 270 nm is increasing as the time goes, which indicates that another reaction is happening. Based on the information from previous published work,^[40] it can be understood that this process is polymerization of phenol. The extent of polymerization can be seen in figure 23. After 300 minutes, it could reach nearly 14 % (the final increased fraction of the absorbance at 270 nm) of polymerization, which can be seen as the negative effect or competing effect to photocatalytic decomposition of phenol.

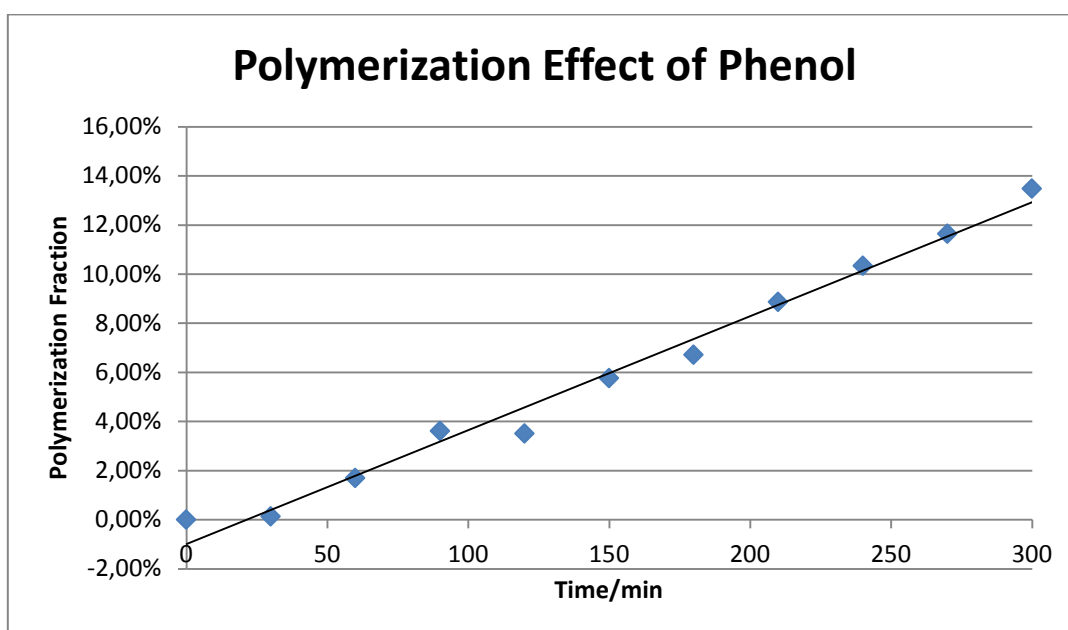


Figure 23. Polymerizaion effect of phenol solution under UV light.

Photocatalytic activity measurements

As illustrated above, 0.1 mM phenol aqueous solution was used to evaluate the photocatalytic activities of mesoporous TiO₂ films. Figure 24 shows the UV-Vis spectra of the phenol containing solution exposed to the mesoporous TiO₂ film prepared from a microemulsion aged in the oven for 96 hours. The concentration of phenol during the reaction was measured every 30 minutes and 300 minutes in total. The peaks at 210 nm and 270 nm drops very fast as the reaction continues. This indicates that the photocatalysis reaction can degrade the phenol under UV-Visible light efficiently and might also be able to inhibit the polymerization effect at the same time. It can be also speculated that with enough time, this amount of phenol

can be completely decomposed if the oxygen in the solution is still enough to sustain the photocatalysis reactions.

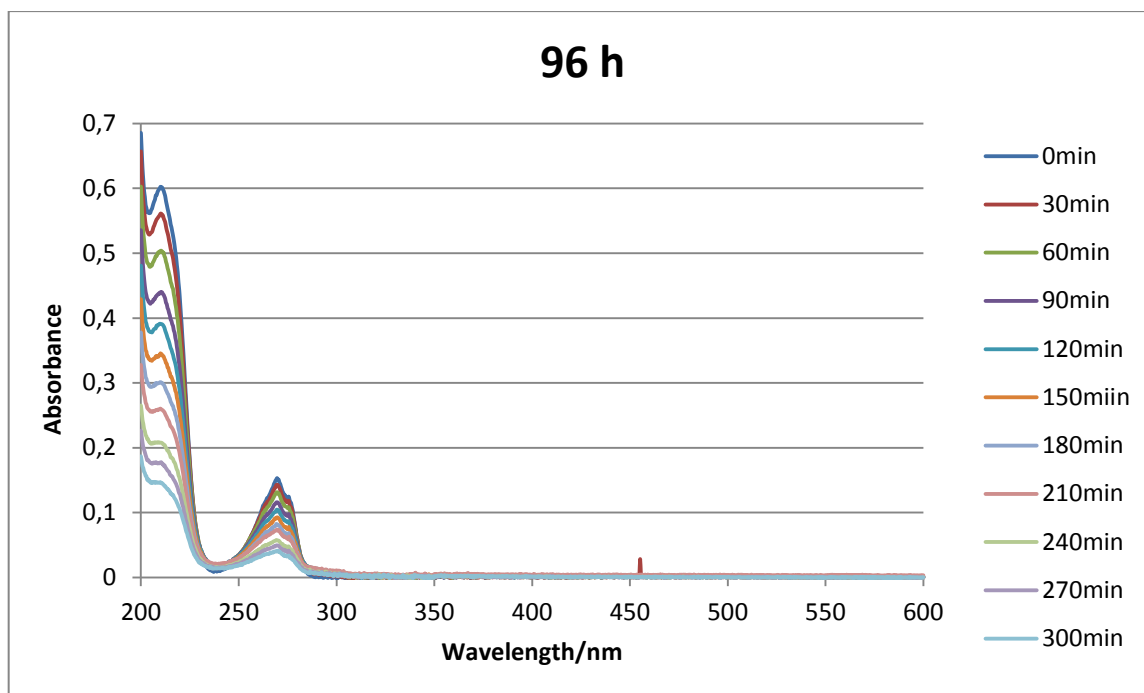


Figure 24. UV-Vis spectra of phenol decomposition over the mesoporous TiO_2 film prepared from a microemulsion aged at 40°C for 96 hours.

Figure 25 shows the photocatalytic activities of mesoporous TiO_2 films with their microemulsions aged for 1 h, 3 h, 6 h, 12 h, 24 h, 48 h, and 96 h in the oven at 40°C individually. The photocatalytic activity here is measured through dividing the amount of phenol degraded by the mass of TiO_2 films that was in contact with the phenol solution. Samples after aging for 1 h, 3 h, 6 h, 12 h, 24 h, 48 h contains similar size of crystallite which varies from 2-5 nm. However, the content of the crystallites in the materials increases as the aging process lasts for longer time, more amorphous TiO_2 will transform to crystalline TiO_2 , and more lights can be absorbed, and thus larger amounts of reactive species can be formed. In this case, the sample aged for 1 h has the lowest photocatalytic activity and the photocatalytic activity continuously and dramatically increases for the samples that have longer aging time. After aging for a long enough time, the crystallite grows even bigger, for sample after aging 96 h, it contains the most crystallites and the crystallites size also reaches 10 nm, which result in a smaller bandgap and higher light absorbance, leading to a much better photocatalytic activity. In general, the photocatalytic activity of mesoporous TiO_2 has a linear relation with aging time of the microemulsion. This might be due to the increasing

content of crystallite and quantum size effect of nanomaterials when the crystallite size grows up. The scatter of the data points probably is because of the error from weighing the films. The results reveal that the photocatalytic activity could be affected by the content and size of the crystallites, but it does not have a direct relation with the order of the mesoporous structure. Even if the pores are not in an ordered arrangement, their surface area could still be as large as the ordered mesoporous structure.

	1 h	3 h	6 h	12 h	24 h	48 h	96 h
Degradation Fraction	28,70%	30,20%	37%	27,50%	35,90%	51,20%	73,30%
Mass/mg	0,48	0,49	0,58	0,44	0,5	0,39	0,4

Table.1. Degradation fraction of phenol after 300 minutes of UV exposure and mass of TiO₂ films with their microemulsions aged at 40 °C for different length of time.

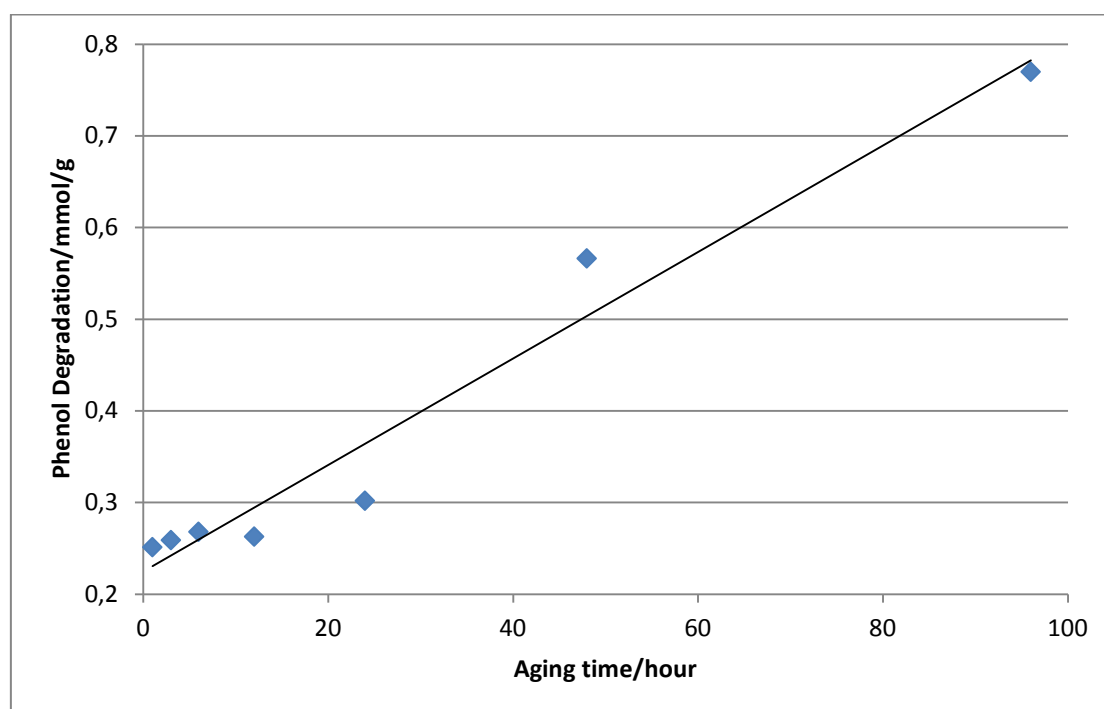


Figure 25. Photocatalytic conversion of phenol after 300 minutes of UV exposure of mesoporous TiO₂ films with their microemulsions aged at 40 °C for different periods of time normalized to the amount of photocatalyst used.

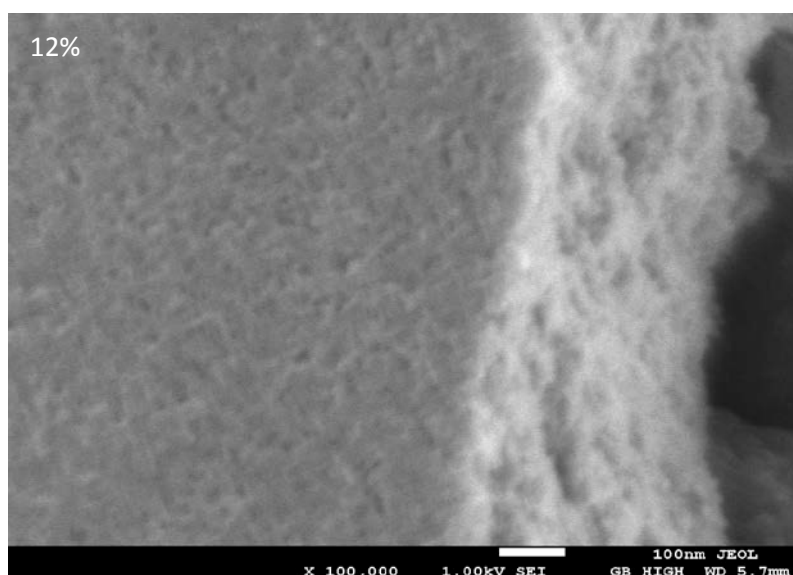
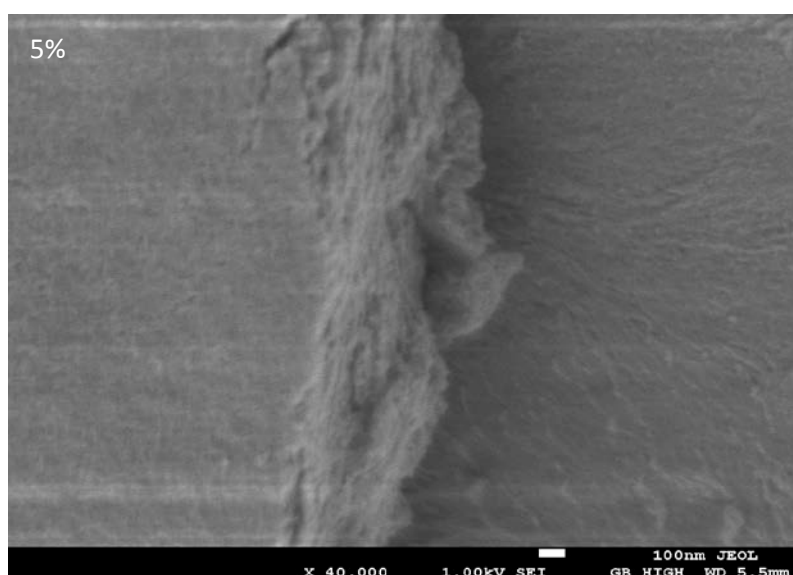
Humidity Series

5%, 12%, 45%, 75%, 98% relative humidity environments for aging phase of the TiO₂ thin films were created by introducing SiO₂ gel, saturated aqueous solutions of LiCl, K₂CO₃, NaCl, K₂SO₄, respectively in a sealed box in order to study how the humidity affects the

morphology and photocatalytic activities of the TiO₂ films. All the microemulsion systems were aged in the oven for 6 hours before fabricating thin films.

Morphology

The morphology of TiO₂ thin films aged at different relative humidity was first studied by SEM (see figure 26). Samples aged at relative humidity of 5% does not show obvious mesoporous structure. Samples aged at relative humidity from 12% to 75% all show mesoporous structure, but only the sample aged at 75% relative humidity gives hexagonal arrangement of pores, and the channels are also well aligned. It can be clearly concluded that the order of the mesoporous structures improves when higher humidity was introduced during the aging period of TiO₂ films.



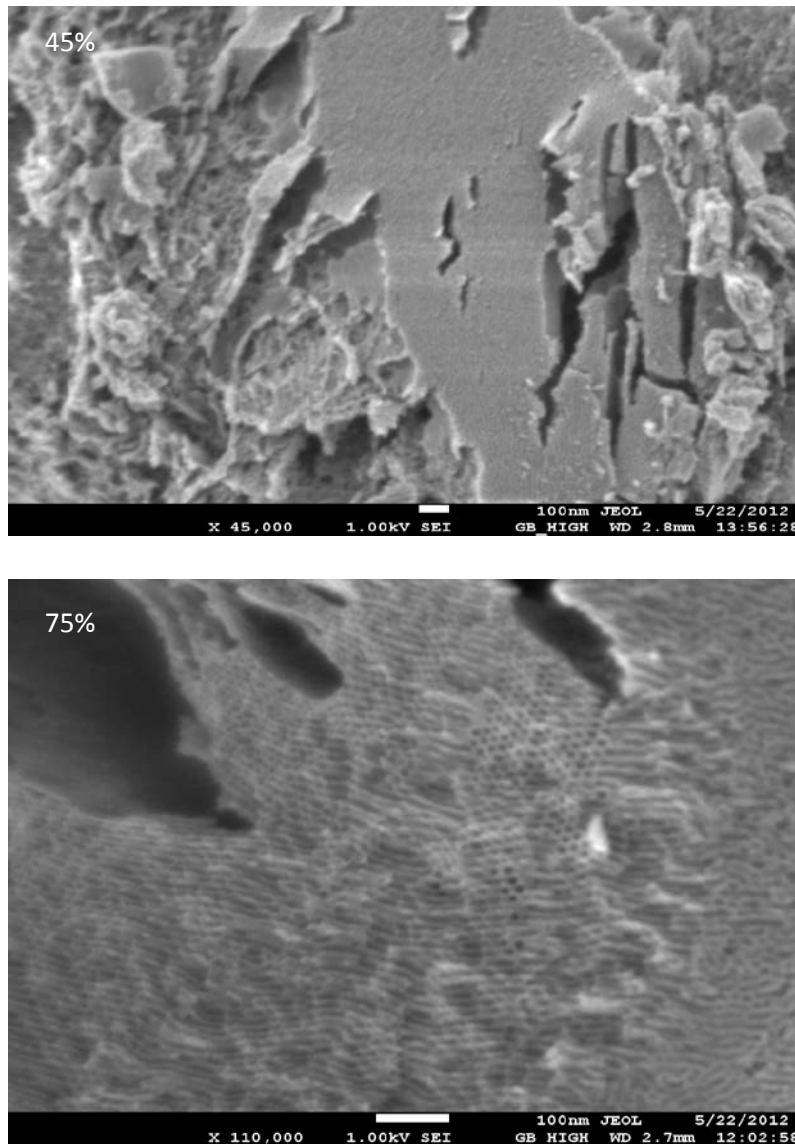


Figure 26. SEM images of TiO₂ films aged at different relative humidity.

GISAXS was also applied here with the purpose to further achieve specific information about the morphology of TiO₂ mesoporous films. Figure 27 shows the cuts of 2D GISAXS data in horizontal direction taken at the Yoneda peak of TiO₂ films for the whole humidity series. q_z is the direction that is perpendicular to the surface.^[45] From the bottom to the top, the humidity environments for aging of TiO₂ films start from the lowest relative humidity of 5% to the highest relative humidity of 98%. Theoretically the higher the sharper the turning point is, the better the order can be predicted. By comparing the intensity and the shape of the curve for the different samples, it can be concluded that the order of mesoporous structures of TiO₂ films increases as the relative humidity for aging phase increases.

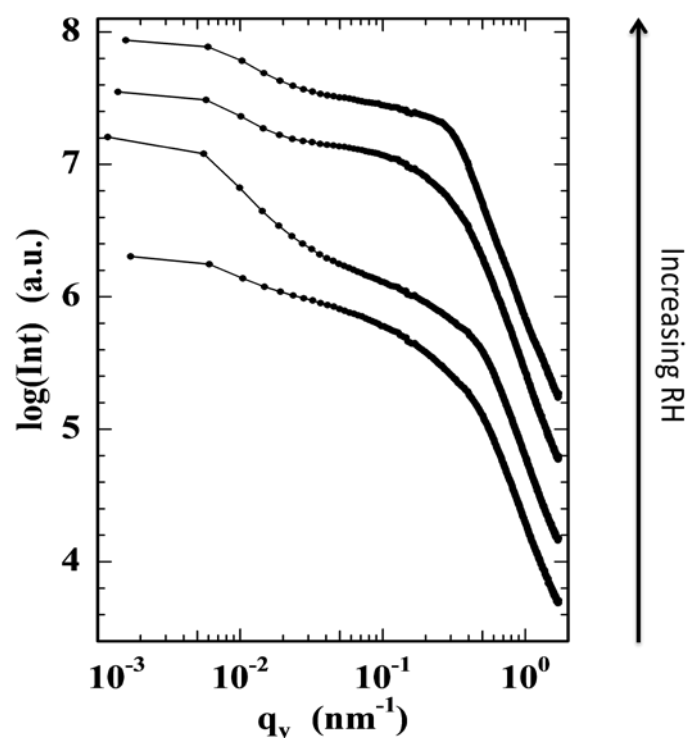


Figure 27. Cuts of 2D GISAXS data in horizontal direction taken at the Yoneda peak of TiO₂ for the whole humidity series.

By analyzing the X-ray intensity of GISAXS measurement and the Yoneda peak positions, the density of mesoporous TiO₂ films can be studied, which can help to verify the porosity of TiO₂ films. The results are shown in the left picture of figure 28. When the relative humidity was 5%, the density of the film is the highest, about 3.45 g/cm³, which corresponds to the lowest porosity. The density decreases a lot when the humidity increases to 12% and the density's decreasing tendency continues when the relative humidity reaches 45%. After that, the value of density stays at a rather constant level which is about 2.3 g/cm³ when the relative humidity is increased further. This indicates that the relatively higher humidity (above 45%) during the aging phase gives increased porosity, which could also mean larger specific surface area and more active sites for the photocatalytic reactions. The right picture of figure 27 provides information about the size of the pores (red dots) derived from the GISAXS data. The radius of the pores is calculated from a model assuming cylindrical pores. The radius is in good agreement with HR-TEM micrographs of the same samples. As the relative humidity increases, from 5% to 75%, the radius of the pores also increases slightly, from 2.5 nm to 4.0 nm. This is also consistent with the result from previous work.^[17] Then the radius declines to 2.8 nm when the relative humidity reaches 98%. These two measurements illustrate the relations between relative humidity of the aging phase for TiO₂ films and their porous

structure. Generally the higher the humidity is applied, the higher the porosity and bigger size of pores can be achieved, which may also result in higher specific surface area. The reason for this phenomenon is probably because the substantial amount of water must be introduced in order to ensure the necessary fluidity that allows the organization of the template in the liquid crystal phase.^[46]

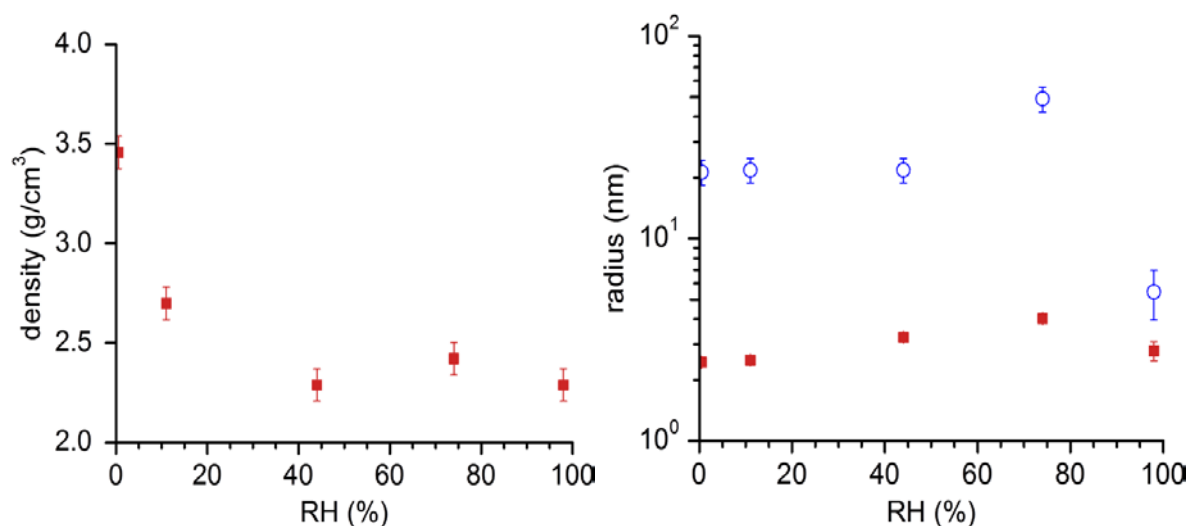


Figure 28. (left) Density of TiO₂ films aged at different humidity environments. (right) Radius of pores for the same series of TiO₂ films.

Figure 29 shows the TEM images of TiO₂ films aged at 5% and 75% relative humidities. It has been realized that the film aged at 5% relative humidity does not show an ordered mesoporous structure, and the film aged at 75% relative humidity shows the ordered hexagonal mesoporous structure, which also corresponds to the previous series of films discussed. From the TEM images it can be recognized that the film aged at 5% relative humidity has very little amount of crystallites with size about 5 nm and with large parts still remaining amorphous. While the film aged at 75% relative humidity contains much higher amount of crystallites, which also corresponds to the results of the previous series.

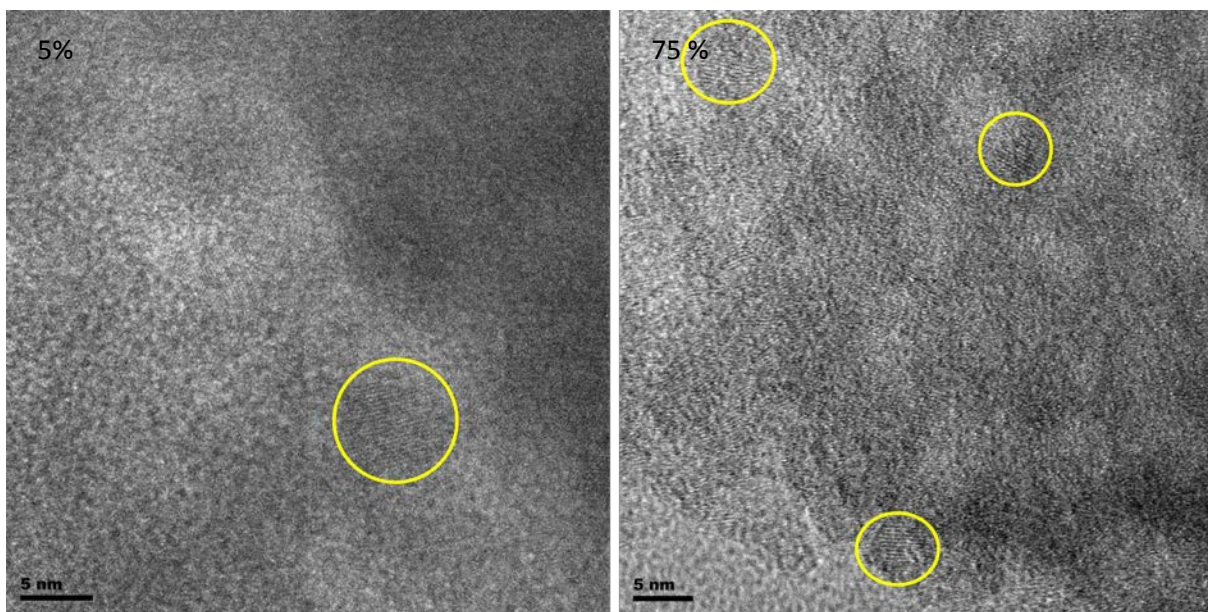


Figure 29. TEM images of TiO₂ films aged at 4.5% and 75% relative humidity.

Taking into account all the morphology studies above about the humidity series, it can be realized that the lower humidity environments, such as 5% and 12% relative humidities, result in lower ordered mesoporous structure. This might be because that lower humidity increases the rate of the condensation process. The water is one of the products from the condensation and the lack of water leads the reaction to proceed faster, which may result in a too fast process, and the TiO₂ polymeric molecules does not have time to relax and arrange in the form of crystallites. There might also be too little time for the surfactant molecules to rearrange and form a liquid crystal. With higher humidity environment, such as 45% and 75% relative humidities, the rate of the condensation reaction slows down and gets optimum. This provides more time for the molecules to organize and form crystallites. Another thing that is worth to be noticed is that since the film aged at 5% relative humidity gives lower content of crystallite and film aged at 75% relative humidity gives higher crystallite content. It has been reported that water could affect the onset of crystallization.^[47] This indicates that the formation of crystallites can happen and be affected both by the aging phase for the microemulsion in the oven, and the aging phase for the TiO₂ films in certain humidity environment, and they are controlled by different parameters.

UV-Vis transmission measurements

UV-Visible light transmission has been measured to detect the content of the crystallite of our materials. Figure 30 shows the transmission of ultraviolet and visible light after passing

through the TiO₂ thin films aged at different humidity environments. The curves of films aged at 5% and 75% relative humidity environments are considered as the references combining the information achieved from TEM images above. It clearly can be seen that the position of the curve for sample aged at 12% relative humidity is slightly lower than the curve for sample aged at 5% relative humidity, and their shapes are close. This indicates that these two samples probably contain similar amounts of crystallites, which is low. However, it still can be predicted that the sample aged at 12% may still contain a slightly higher amount of crystallites. The sample aged at 45% relative humidity also exhibits a similar curve with the sample aged at 75% relative humidity. This also indicates that these two samples contain similar amounts of crystallites, which is high, but the sample aged at 45% relative humidity may contain a little bit less crystallites by considering its slightly higher curve than the other. When humidity increases from 5% to 75%, the curves continuously shift toward the longer wavelength area, which is closer to the visible area. This may also indirectly prove the increasing content of crystallites, because the band gap of the crystalline TiO₂ is smaller than the amorphous TiO₂. Light with lower energy could be absorbed by TiO₂ crystallites.

The sample aged at 98% was not able to analyze with UV-Visible absorbance because the film was in liquid state during the aging phase at this humidity, which resulted in an uneven film, so it was impossible to measure this sample due to the different thickness at different parts of the film.

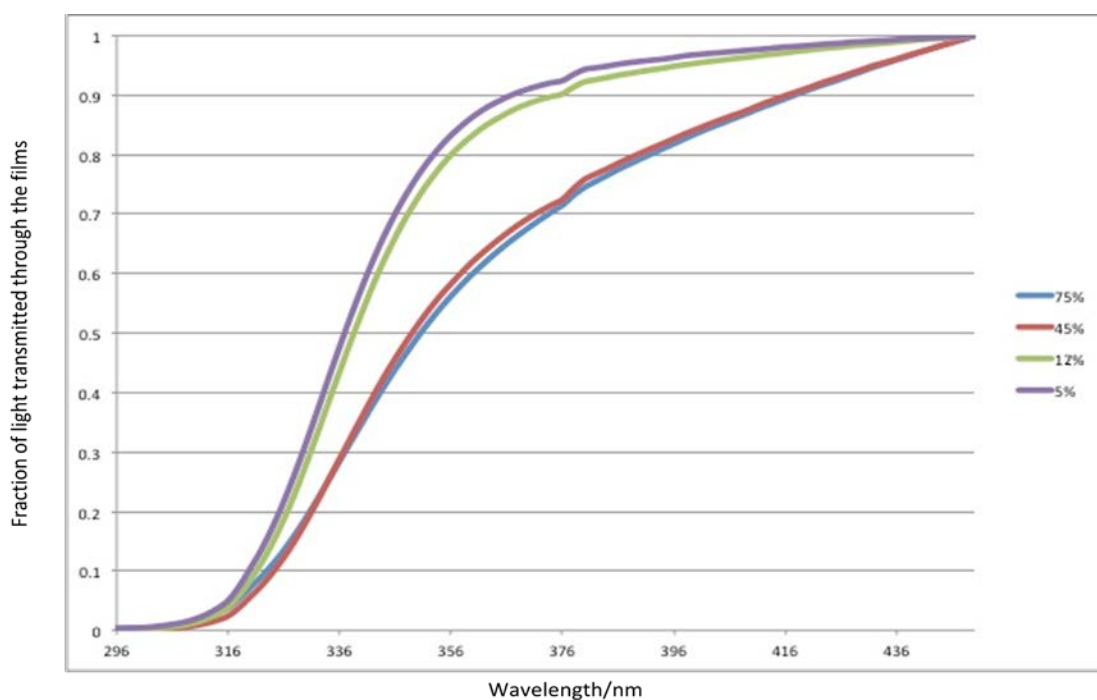


Figure 30. UV-Visible light transmission of TiO₂ films aged at different humidity environments

Photocatalytic activity measurements

The photocatalytic activity of the humidity series was investigated and the results are displayed in figure 31 and figure 32. All the samples were measured at the same conditions and with same methods as the previous series. Figure 31 shows the phenol fraction in the reactor of the whole experimental process. The different curves represent different samples aged at different humidity environments. It can be seen here that the fraction of phenol decreases very slowly for the sample aged at 5% relative humidity, this corresponds to its lower content of crystallites and possibly smaller crystallite size which results in a larger band gap. Very little energy can be absorbed by this sample. In the beginning phase, the signal of phenol even slightly increases and this lasts for 120 minutes, which may demonstrate that the very little amount of crystallites present is not able to inhibit the polymerization of phenol in the beginning. As the humidity increases, the slopes get steeper, which means the degradation process goes faster and is more effective. This phenomenon also corresponds to the increasing content of crystallites and the decrease of the band gap for samples aged at higher humidity environments as discussed before. More light can be absorbed and more energy can contribute to the photocatalytic effect in this case. The degradation starts from the beginning of the measurements, this means the photocatalytic activities are high enough to inhibit the polymerization of phenol from the beginning. These results also prove that even light with wavelength below 300 nm can still cause polymerization of phenol, and only the sample with good enough activity can inhibit this negative effect.

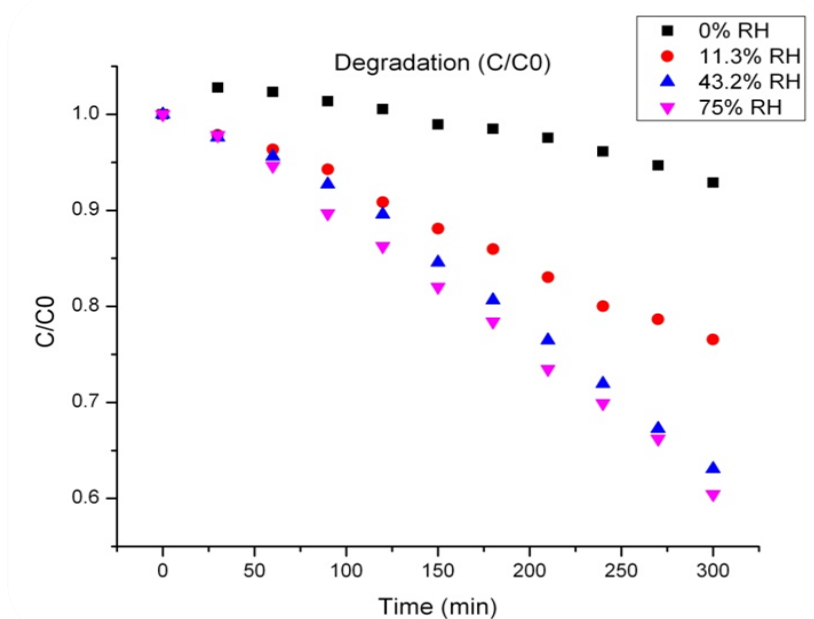


Figure 31. Phenol decomposition of the whole reaction process photocatalysed by TiO₂ films aged at different humidity environments.

The final phenol fraction after being photocatalytically degraded for 300 minutes can be seen in figure 32. The sample aged at the lowest humidity gives the smallest degradation of phenol, only less than 5%. When the humidity increases to 12%, there is a big improvement for the degradation, which reaches 23%. A similar improvement happens for the sample aged at 45% relative humidity. The sample aged at 75% relative humidity exhibits the best degradation ability, 40% degradation of phenol. However, the improvement from relative humidity of 45% to 75% is not as big as others, this may be because the sample aged at 45% relative humidity already has achieved fairly good order of the pores from the data of GISAXS and similar content of crystallites compared to the TiO₂ film aged at 75% relative humidity. Then the density and porosity are also quite close for these two TiO₂ films. The increase of photocatalytic activity for the sample aged at 75% relative humidity might be mainly due to the slight increase of the content of crystallites.

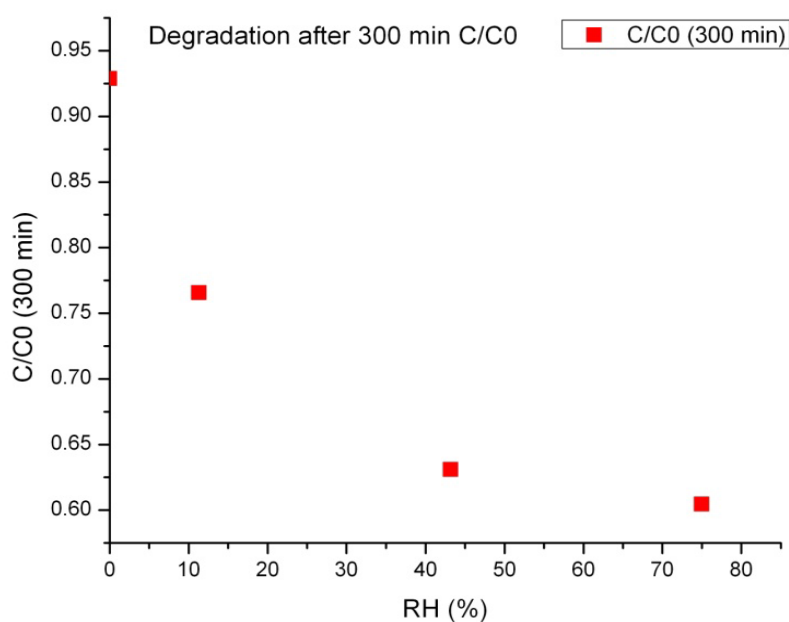


Figure 32. Final fraction of phenol decomposition photocatalyzed by TiO₂ films aged at different humidity environments.

Fe dopant series

The content of 0.4%, 0.8%, 1.2%, 1.6% weight fraction of Fe dopant was introduced during the process of synthesizing the microemulsions with the same compositions and they were all aged in the oven at 40 °C for 12 hours. TiO₂-Fe films were aged in sealed buckets containing saturated NaCl aqueous solution for over two days.

Photocatalytic activity measurements

Figure 33 shows the results of the photocatalytic activity measurements with different content of Fe dopant after irradiation for 300 minutes with the same setup and same intensity of light as used in the experiments presented before. The sample without Fe dopant was used as the blank reference. It can be seen that when the weight fraction of Fe is 0.4%, the amount of phenol degraded reaches 37% compared to the film without dopant which is 27.5%. However, when increasing the content of Fe to 0.8%, the degradation of phenol decreases to 20%, which is even lower than the TiO₂ film without dopant. When further increasing the content of Fe, the degradation of phenol continuously diminishes. This result indicates that a proper amount of Fe dopant can improve the photocatalytic activity of TiO₂ films because dopant can replace Ti and create band between valence band and conduction band of titania, which enhances the excitation of electrons. More light with longer wavelength can be absorbed in this condition. A small amount of Fe³⁺ can also act as electron scavengers which can enhance the charge separation.^[26] The content of dopant in this case should be quite small in order to achieve optimum improvement. The reason for the negative effect of higher content of iron dopant might be because of the dramatically decreasing crystallite size in the TiO₂ films as the content of iron dopant increases.^[48]

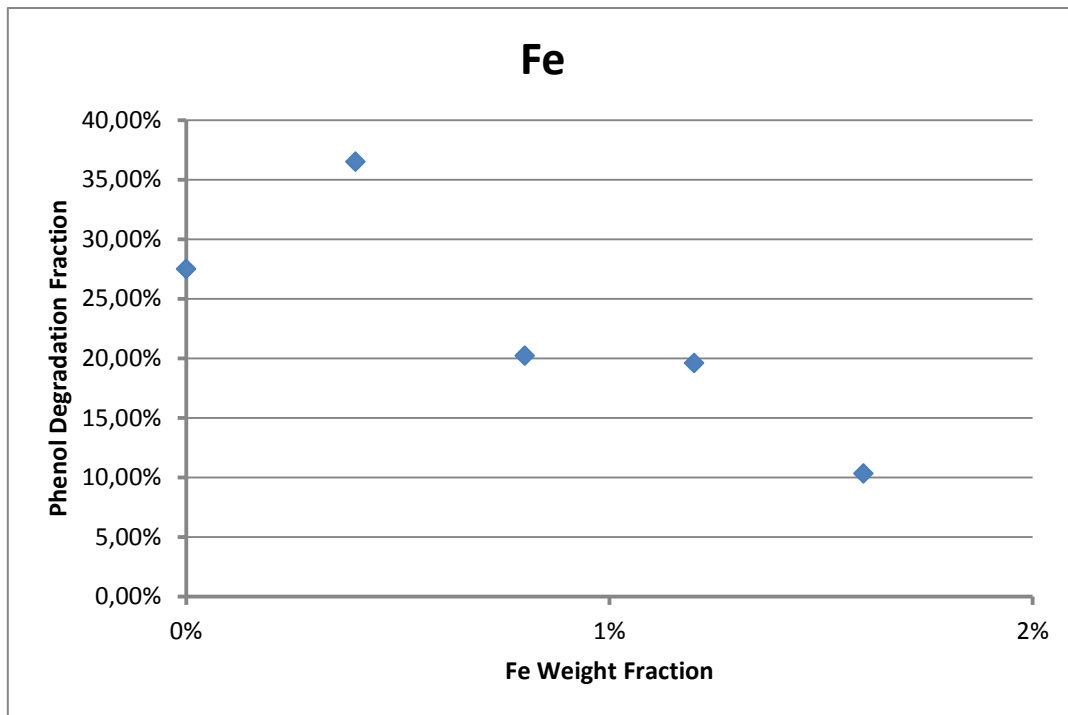


Figure 33. The effect of differet amounts of iron dopant to the photocatalytic activity of TiO₂ films.

Conclusions

1. Mesoporous TiO₂ thin films were successfully synthesized via this microemulsion system at low temperature.
2. Aging time of microemulsion in the oven at 40 °C could affect the formation of crystallites and morphology of the final TiO₂ films. The content of crystallites kept increasing as the aging time was prolonged, and the films performed higher photocatalytic activities. The size of the crystallites was below 5 nm when the aging time was below 48 hours, which contributed to form mesoordered structures for TiO₂ films. After aging for 96 hours, the crystallite size grew up to 10 nm, which could not sustain mesoordered structure. Order of the mesoporous structures did not show direct relations to photocatalytic activity.
3. Increasing humidity for aging TiO₂ films (from 5% to 75%) generally increased the order of the mesoporous structure, content of crystallites, porosity and the size of the pores. The last three factors improved the photocatalytic activities of TiO₂ films.
4. Very small amounts of iron dopant could improve the photocatalytic activity of the TiO₂ films. However, relatively higher amounts of dopant reduced the photocatalytic activities, possibly by means of reducing the size of the crystallites.

Future work

The effect of iron dopant could be further studied in order to find out the optimal weight fraction to improve the photocatalysis and study the mechanisms for its negative effect when iron dopant is added in too high amounts. The morphology, crystallization of TiO₂-Fe films and their molecular structures could also be investigated.

Acknowledgement

I'd like to thank Professor Anders Palmqvist to provide me this great opportunity to join his research group and work on this interesting project, as well as his inspirations and suggestions during this whole year. Thanks to Björn Esbjörnsson for patiently teaching me how to do research work based on this amazing material including synthesis, characterizations and analysis of the results. I also appreciate Professor Krister Holmberg for his guidance of microemulsion and the behaviors of surfactants, and all the people working at Applied Surface Chemistry for their generous help and support through this whole year. Prof. Peter Müller-Buschbaum, Lehrstuhl für Funktionelle Materialien, Physik-Department, Technische Universität München, Germany and his co-workers are gratefully acknowledged for their support in carrying out the GISAXS measurements and analyses. Prof. Osamu Terasaki, Graduate School of EEWS (WCU), KAIST, Republic of Korea and his co-workers are gratefully acknowledged for their support in carrying out the TEM and SEM analyses. Finally, I would like to thank my friends Oscar Lidström and Ye Li for sharing this wonderful time together at Applied Surface Chemistry and my family for their unconditional support and love.

References

- [1] Laoufi, N.A.; Tassalit, D.; Bentahar, F. *Global Nest Journal* 2008, 10, 404.
- [2] Pellizzetti E.; Macrino V.; Minero C.; Carlin V.; Pramauro E.; Zerbinati O.; Tosano M.L. *Environ. Sci. Technol.* 1990, 24, 1559.
- [3] Galze H.; Beltran F.; Tuhkanen T. Kang J.W. *Water Poll. Res. J. Canada* 1992, 27, 23.
- [4] Mirat D.G.; Vatistas R. *Water Research* 1997, 21, 895.
- [5] Esplugas S.; Yue P.L. Perez M.I. *Water Research*, 1994, 28, 1323.
- [6] Keidel E.; Zeitung F. 1929, 34, 1242.
- [7] Fujishima A.; Honda K. *Nature* 1972, 238, 37.
- [8] Hashimoto K.; Irie H.; Fujishima A. *Japanese Journal of Applied Physics* 2005, 44, 8269.
- [9] Antonelli, D. M.; Ying, J. Y. *Chem. Mater.* 1996, 8, 874.
- [10] Ulagappan, N.; Rao, C. N. R. *Chem. Commun.* 1996, 1685.
- [11] Lee, J. K.; Kim, G. P.; Song, I. K.; Baeck, S. H. *Electrochem. Commun.* 2009, 11, 1571.
- [12] Pokhrel, S.; Simion, C. E.; Teodorescu, V. S.; Barsan, N.; Weimar, U. *Adv. Funct. Mater.* 2009, 19, 1767.
- [13] Nilsson E. Ph.D. Thesis, Chalmers University of Technology
- [14] Hoffmann, M. R.; Martin, S. T.; Choi, W. Y.; Bahnemann, D. W. *Chem. Rev.* 1995, 95, 69.
- [15] Alberius, P. C. A.; Frindell, K. L.; Hayward, R. C.; Kramer, E. J.; Stucky, G. D.; Chmelka, B. F. *Chem. Mater.* 2002, 14, 3284.
- [16] Choi, S. Y.; Mamak, M.; Coombs, N.; Chopra, N.; Ozin, G. A. *Adv. Funct. Mater.* 2004, 14, 335.
- [17] Nilsson E.; Sakamoto Y.; Palmqvist A.E.C. *Chem. Mater.* 2011, 23, 2781.
- [18] Holmberg K.; Jönsson B.; Kronberg B.; Lindman B. *Surfactants and Polymers in Aqueous Solution*, 2nd edition.
- [19] Figure taken from lecture notes in the course Surface Chemistry (KTK095), Chalmers University of Technology, 2010.
- [20] <http://www.chm.bris.ac.uk/webprojects2001/hoets/mesoporouswebpagehome.htm>
- [21] Smart L.E.; Moore E.A. *Solid state chemistry*, Third Edition.
- [22] <http://mrsec.wisc.edu/Edetc/background/LED/band.htm>
- [23] http://www.nanolytics.de/index.php?lg=en&main=field_of_business&sub=why_colloids
- [24] Pedersen K. Quantum size effects in nanostructures.

- [25] Akurati K.K. Synthesis of TiO₂ based nanoparticles for photocatalytic applications.
- [26] Naeem K.; Ouyang F. *Physica B* 2010, 405, 221.
- [27] Wellia D.V.; Xu Q.C.; Sk M.A.; Lim K.H.; Lim T.M.; Thatt T.; Tan Y. *Applied Catalysis A: General* 2011, 401, 98.
- [28] Colo'n G.; Maicu M.; Hidalgo M.C.; Naví'o J.A. *Applied Catalysis B: Environmental* 2006, 67, 41.
- [29] Choi H.; Antoniou M.G.; Pelaze M.; Delacruz A.A.; Shoemaker J.A.; Dionysiou D.D. *Environ. Sci. Technol.* 2007, 41, 7530.
- [30] Livraghi S.; Paganini M.C.; Giamello E.; Selloni A.; Valentin C.D.; Pacchioni G. *JACS* 2006, 128, 15666.
- [31] Chen D.; Jiang Z.Y.; Geng J.Q.; Wang Q.; Yang D. *Materials and Interface* 2007, 46, 2741.
- [32] Bingham S.; Daoud W.A. *Journal of Material Chemistry* 2010, 21, 2041.
- [33] Okamoto K.I.; Yamamoto Y.; Tanaka H.; Tanaka M. *The Chemical Society of Japan* 1985, 58, 2015.
- [34] Xiong L.; Zheng L.Z.; Xu J.P.; Zheng D.; Li J.H.; Li X.J.; Sun J.; Liu Q.; Niu L.L.; Yang S.M.; Xia J. *Environ Chem Lett.* 2011, 9, 251.
- [35] <http://www.chemistry.adelaide.edu.au/external/soc-rel/content/beerslaw.htm>
- [36] Yang G.B.; Yu L.G.; Chen X.H.; Zhang P.Y. *Applied Surface Chemistry* 2009, 255, 4097.
- [37] Dahl S.; Eriksson P.; Nordström P.; Sassi U.; Sandin G.; Yuan N. *Project in Nanomaterials Chemistry (KTK041)*, Chalmers University of Technology, 2010.
- [38] http://en.wikipedia.org/wiki/File:Scheme_TEM_en.svg
- [39] Figure taken from lecture notes in the course *Nanomaterials Chemistry (KTK041)*, Chalmers University of Technology, 2010.
- [40] <http://www.gisaxs.de>
- [41] <http://staff.chess.cornell.edu/~smilgies/gisaxs/GISAXS.php>
- [42] Salditt M.R.; Spohn H. *Phys. Rev. B.* 1995, 52(23), 16855.
- [43] Holmqvist P.; Alexandridis P.; Lindman B. *J. Phys. Chem. B* 1998, 102, 1149.
- [44] Hu C.; Wang Y.Z.; Tang H.X. *Chemosphere* 2000, 41, 1205.
- [45] Niedermeier M.A.; Magerl D.; Zhong Q.; Nathan A.; Körstgens V.; Perlich J.; Roth S.V.; Buschbaum P.M. *Nanotechnology* 2012, 23, 145602.
- [46] Crepaldi E.L.; Soler-Illia G.J.; Grosso D.; Cagnol F.; Ribot F.; Sanchez C. *JACS* 2003, 125, 9770.
- [47] Bass J.D.; Grosso D.; Boissiere C.; Sanchez C. *JACS* 2008, 130, 7882.

[48] Ada'n C.; Bahamonde A.; Ferná'ndez-García M.; Martí'nez-Arias A. *Applied Catalysis B. Environmental* 2007, 72, 11.